



Norwegian University of
Science and Technology

The Biocompatibility and Osteogenic Properties of Additive Manufactured Porous Ti-6Al-4V Scaffolds

Kristin Sirnes Ødegaard

Mechanical Engineering

Submission date: June 2018

Supervisor: Jan Torgersen, MTP

Co-supervisor: Marita Westhrin, EXT

Norwegian University of Science and Technology
Department of Mechanical and Industrial Engineering

Acknowledgement

When I first started to work on this thesis, I had never seen a living cell before and I barely even knew what a cell really was. Since then, I have learned so much within the field of biomedical engineering, and for that I am very grateful.

First and foremost, I would like to thank my supervisor, Associate Professor Jan Torgersen, and co-supervisor, Dr. Marita Westhrin.

Jan, thank you for always keeping your door open and teaching me things I never even knew about. Your input throughout this semester has always been really helpful. In addition, I would like to thank you for hosting the Thursday meetings with the MDC group. These meetings have been really informative, and it has been interesting to see what other students and candidates have been working on.

Marita, to this day, I still wonder why you agreed to teach me all the things you have taught me in the cell laboratory. Thank you for being so patient and explaining me all the things I now know from you, and for answering all the questions I have asked you throughout the semester. I truly enjoyed working with you and learning from you. Also, I am very grateful for the writing input you have given me during the project.

Thank you to the both of you, I feel very privileged for having you two as my supervisor and co-supervisor. I look forward to work more with you for the upcoming three years.

I would also like to thank Professor Filippo Berto. Thank you for always taking the time to answer my questions and for giving me input during this thesis. I would also like to thank you for hosting the Thursday meetings in collaboration with Jan.

Finally, I would like to thank Associate Professor Christer Westum Elverum. Christer, I was introduced to you in the middle of the semester, and since then you have shown interest in this work and given me useful input. I am also grateful that you have given me the trust for future work in this topic with signing me for a PhD position.

Abstract

Human bone is constantly being remodeled, and has the ability to repair itself when damage occurs. However, sometimes the fractures are so intense that they exceed the critical non-healable size. In order to repair such fractures, external fixation, such as implants, may be required.

Titanium and its alloys have, for a long time, been used as solid implants to repair bone damages. These alloys have the ability to form an interlocking bond with human bone. However, due to the big difference in stiffness between the solid titanium implant and human bone, resorption of bone might occur, which eventually might lead to implant failure.

By implementing additive manufacturing, one can produce porous metal implants, with an elastic modulus designed to mimic the stiffness of human bone. This can eliminate the risk of bone resorption and pave the way towards a long lasting prosthetic implant. However, it is still uncertain how much additive manufacturing and porous structures might affect the biocompatibility and osteogenic properties of the implant.

This thesis describes the *in vitro* investigation of the biocompatibility and osteogenic properties of additive manufactured porous scaffolds. The scaffolds were designed with a pore- and lattice diameter of 800 μm , and a porosity of $\sim 60\%$. The scaffolds were manufactured using electron beam melting (EBM) by employing the alloy Ti-6Al-4V. In order to find the biocompatibility, the scaffolds were seeded with bone marrow-derived mesenchymal stromal cells (BMSC). Immediately after being seeded, the cells adhered to the surface of the scaffolds, and subsequently proliferated. This infers that EBM manufactured scaffolds are biocompatible.

The osteogenic potential of BMSC cultured on the scaffolds was studied using ALP- and ARS-staining and gene expression analysis. Results from ALP and ARS analysis inferred that the BMSC became mature, functional osteoblasts, when cultured in osteogenic medium.

Sammendrag

Når et benbrudd oppstår, så reagerer kroppen umiddelbart med å reparere skadene. Dette gir bein muligheten til å ombygge seg selv for å reparere skader. Noen ganger er bruddene så store at de overstiger den kritiske ikke-helbredelige fasen. Slike brudd kan repareres ved å ta i bruk for eksempel implantat.

Titan og dens legeringer har lenge vært brukt til solide implantater, for å reparere store beinskader. Titanlegeringer har evnen til å danne en integrasjon mellom metallens overflate og benet. Titan har, derimot, en veldig høy stivhet sammenlignet med bein. På grunn av den store forskjellen i stivhet, så kan det resultere i at benet løsner fra implantatet.

Ved å introdusere additivproduksjon, så kan porøse metallimplantater bli produsert. Disse kan modelleres med en elastisk modul som er utformet for å etterligne stivheten av bein. Dette vil eliminere risikoen for at bencellene løsner fra implantatet, og vil dermed bane vei mot et langvarig implantat. Det er imidlertid fremdeles usikkert hvor mye additivproduksjon og porøse strukturer kan påvirke biokompatibiliteten og de osteogene egenskapene til implantatet.

Denne oppgaven beskriver de *in vitro* undersøkelsene som ble gjort for å finne biokompatibiliteten og de osteogene egenskaper hos additiv produserte porøse skaffolder. Disse skaffoldene ble utformet med en pore- og struktur diameter på 800 μm , og en porøsitet på $\sim 60\%$. Skaffoldene ble fremstilt ved hjelp av elektronstrålesmelting (EBM) med legeringen Ti-6Al-4V. For å finne biokompatibiliteten, så ble skaffoldene sådd med beinmargceller (BMSC). Straks etter at de ble sådd med celler, så adhererte cellene seg til overflaten av skaffoldene, og cellene begynte deretter å proliferere. Dette resultatet viste at EBM-produserte skaffolder er biokompatible.

Det osteogene potentialet til BMSC kulturert på skaffoldene ble undersøkt ved hjelp av ALP- og ARS-farging, i tillegg til analyse av gennuttrykk. Resultat fra ALP- og ARS-farging viser at skaffoldene stimulerer osteoblastogenese, og at BMSCene som ble dyrket på skaffoldene, differensierer til modne osteoblaster.

Table of Contents

Acknowledgement	iii
Abstract	v
Sammendrag	vii
Table of Contents	xi
1 Introduction	1
1.1 Background	2
1.2 Biomedical Background	2
1.2.1 Bone Structure	2
1.2.2 Osseointegration	5
1.2.3 The Bone Marrow	6
1.2.4 Bone marrow-derived Mesenchymal Stromal Cells	6
1.2.5 Tissue Engineering	8
1.2.6 Gene Expressions	8
1.2.7 Biomedical Challenges	9
1.3 Mechanical Background	11
1.3.1 Additive Manufacturing	11
1.3.2 Selective Laser Melting	11
1.3.3 Electron Beam Melting	12
1.3.4 PBF Powder Characteristics and Production	13
1.3.5 Additive Manufacturing Challenges	13
1.3.6 Biomaterials	14
1.3.7 Titanium-Based Alloys	14
1.3.8 Additive Manufactured Ti-6Al-4V	16

2	Aim of Thesis	17
2.1	Research Background and Motivation	18
2.2	Outline	19
2.3	State of the Art	20
2.3.1	Effects of Pore Size and Porosity, <i>in vivo</i>	20
2.3.2	Effects of Pore Size and Porosity, <i>in vitro</i>	20
2.3.2.1	Mechanical Characteristics	21
2.3.2.2	Metabolic Activity and Adhesion	21
2.3.2.3	Osteoblast Differentiation	24
2.3.2.4	Conclusion	27
3	Experimental Methods	29
3.1	Mechanical Methods	29
3.1.1	Scaffold Design	29
3.1.2	Scaffold Manufacturing	31
3.2	Biomedical Methods	33
3.2.1	Experimental Setup	33
3.2.1.1	Cell Culturing	33
3.2.1.2	Seeding of Cells	34
3.2.1.3	Cell Counting	35
3.2.1.4	Fixation	36
3.2.2	AlamarBlue	36
3.2.3	Alkaline Phosphatase Assay	37
3.2.4	Fluorescence Microscopy	37
3.2.5	PCR Analysis	39
3.2.5.1	RNA Isolation	39
3.2.5.2	cDNA Synthesis and PCR Analysis	40
3.2.6	Alizarin Red Staining	41
4	Results	43
4.1	Manufactured Scaffolds	43
4.2	Metabolic Activity	45
4.3	Alkaline Phosphatase Activity	46
4.4	PCR Analysis	47
4.4.1	Experiment 1	47
4.4.1.1	RNA Concentration	47
4.4.1.2	Collagen Type I	48
4.4.1.3	RUNX2	49
4.4.1.4	Osterix	49

4.4.1.5	Osteocalcin	50
4.4.2	Experiment 2	51
4.4.2.1	RNA Concentration	51
4.4.2.2	Collagen Type 1	52
4.4.2.3	RUNX2	53
4.4.2.4	Osterix	53
4.4.3	Cycle Threshold Values	54
4.5	Alizarin Red Staining	56
5	Discussion	61
5.1	Biocompatibility of Scaffolds	61
5.2	Osteogenic Properties of Scaffolds	62
5.3	Effects of Pore Size and Porosity	65
5.4	Challenges	65
5.4.1	Cell Culturing	66
5.4.2	Microscopy Challenges	68
5.4.3	Cycle Threshold Values	69
6	Conclusion	71
7	Future Research	73
	Bibliography	75
	Acronyms	II
	Glossary	IV
	List of Tables	V
	List of Figures	VIII
Appendix 1		IX
Amplification Plots		IX
Experiment 1		X
Experiment 2		XIII

1 | Introduction

Every person experiences some type of injury during their life. Whether it is a wound, a bone fracture or a burn, the body responds immediately to repair the damages. Bone continually undergoes dynamic biological remodelling. This gives bone the ability to remodel itself to repair damages. However, sometimes the damages are so intense that they exceed the critical non-healable size, and external intervention is required.

Metals and alloys have a long history of applications as bone implants. This include titanium, stainless steels and cobalt based alloys (CoCrMo). In 1952, Per Ingvar Brånemark accidentally discovered that titanium could form an interlocking bond with bone. This process was named *osseointegration*. Since then, titanium and its alloys (Ti-6Al-4V) have been used as dental implants and orthopedic hip implant stems.

Many young patients are receiving these implants, and the required lifespan for the implant must be increased. One of the main challenges with implants is the adaption of their mechanical and biomechanical properties to natural bone. Ti-6Al-4V has a great biocompatibility, satisfactory mechanical strength and excellent corrosion resistance. While the elastic modulus of Ti-6Al-4V is 110 GPa, the elastic modulus of bone is significantly lower, and varies from 0.76 GPa to 34 GPa [1, 2]. Due to the big difference in stiffness between the implant and human bone, then stress shielding might occur, which is a major source for bone resorption.

A successful metallic implant must restore the function of bone and promote regeneration of bone tissue at damage sites. By implementing additive manufacturing in tissue engineering, one can basically achieve the impossible. Porous scaffolds can be manufactured, and the structure and stiffness can be designed in order to resemble human bone. These scaffolds must be characterized with high biocompatibility, surfaces that emphasize proliferation and differentiation, and mechanical properties to match the surrounding tissues to eliminate stress shielding.

1.1 Background

This thesis is an interdisciplinary work, with a combination of both biomedical and mechanical background. The two upcoming sections will therefore explain the necessary background to investigate the biocompatibility and osteogenic properties of additive manufactured porous scaffolds. The biomedical background section will describe the bone structure, the bone remodeling process and the gene expressions that are expected during bone remodeling. It will also describe the specific cell type used for the experimental methods, in addition to osseointegration and tissue engineering. The mechanical background section will include additive manufacturing (AM) and specific types of AM processes. A general explanation of biomaterials will be given and the biomaterial, titanium and its alloys, will be included.

1.2 Biomedical Background

1.2.1 Bone Structure

The skeletal system is described as the infrastructure of the human body, providing a rigid framework that offers protections and support, as well as attachment sites of muscle. Remodeling of bone is a continuous process, and is required during the prenatal period to adulthood, as well as healing bone fractures.

There are four types of bone in the skeletal system. Long bones, short bones, flat bones and irregular bones. Long bones are defined as a bone that is longer than it is wider. Examples of these are the femur, or thigh bone, and humerus. Figure 1.1a shows the structure of the humerus. A short bone is defined as a bone that is as wide as it is long. Examples of these are the bones of the wrists and ankles. Flat bones are broad and flat, for example the cranium. The irregular bones are bones that do not belong in the previous mentioned types, for example the bones of the pelvis and vertebrae (spinal column).

The bone itself consists of two bone types, cortical and trabecular. Cortical bone makes up the outer layer of the bone, and the trabecular bone makes up the inner layer of the bone. While cortical bone is dense and compact, the trabecular bone has a spongy, honeycomb-like structure. Figure 1.1d shows the difference between cortical and trabecular bone. The porosity of trabecular bone ranges from 30 to 90%, and the porosity of cortical bone ranges from 5 to 30%, which makes the mass of the cortical bone roughly four times that of trabecular bone [3].

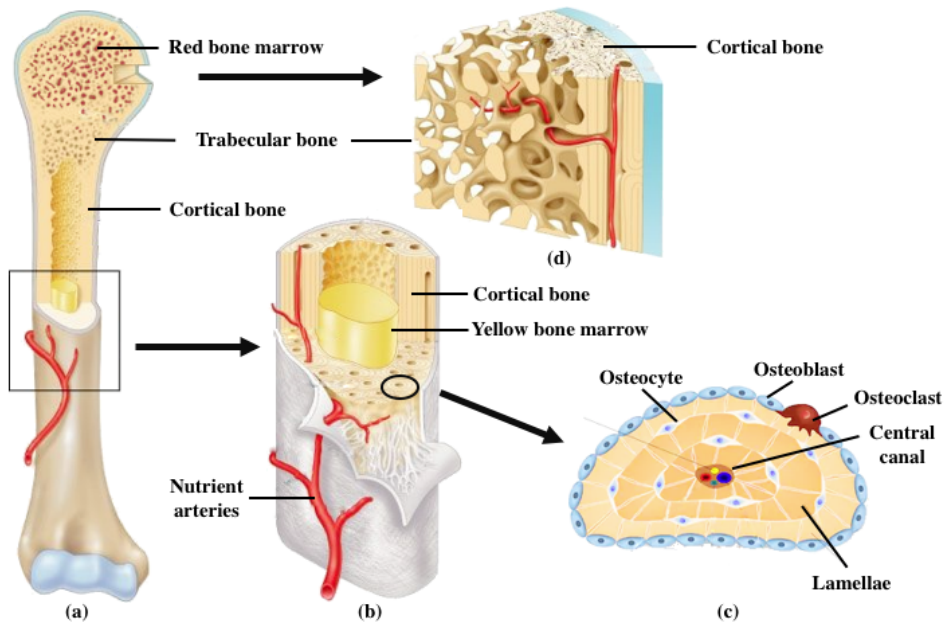


Figure 1.1: The bone structure of a long bone

The figure shows the bone structure of a long bone . Figure (a)¹ shows the structure of a long bone, and figure (b)¹ shows the details inside the shaft of the bone (diaphysis). Figure (c)² shows details of an osteon, and figure (d) shows the details of trabecular and cortical bone.

Bone is mainly composed of collagen, fibers and bone cells. The mechanical properties of bone is affected by the mineral content. Higher mineralization gives stronger and stiffer bone, but it also lowers the ability of absorbing shock and strain energy [3]. The elastic modulus of trabecular bone ranges from 0,76 to 20 GPa [1], and ~34 GPa for cortical bone [2].

Bone modeling is initiated by the differentiation of mesenchymal stem cells. These are cells that have not yet been differentiated into a specific cell type. The mesenchymal stem cells differentiate to the bone forming cells, osteoblasts. During the matrix formation phase that follows, the osteoblasts begin to lay down unmineralized osteoids. Osteoids are the organic part of the bone, consisting of, among others, collagen fibers. The osteoids then get mineralized, and calcifies to form into bone. During bone modeling, the osteoblasts get trapped between the

¹<http://anatomyorgan.com/bone-structure-labeled/bone-structure-labeled-human-long-bone-structure-human-body-diagram/>

²<https://instrideonline.com/bones/>

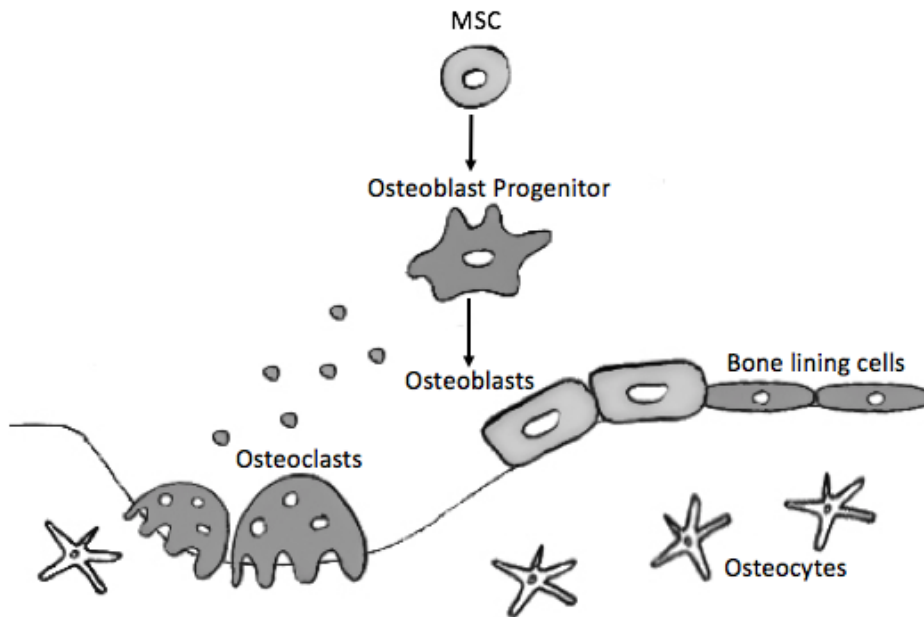


Figure 1.2: Bone (re)modeling

The mesenchymal stem cells have the ability to proliferate and differentiate into osteoblast. Osteoblasts are bone forming cells and differentiate into osteocytes when surrounded by bone matrix. The osteocytes establish contact and communication through a network of cells. From this, the osteocytes are able to respond to mechanical loading. To be able to repair, maintain and remodel the bones, osteoclasts have the function of removing the bone matrix [4]

osteoids, and the osteoblasts are forced to differentiate to osteocytes. In the bone, an interconnected network between the osteocytes is formed, resulting in lamellar bone.

The lamellar bone has a regular, parallel and concentric alignment, as seen in figure 1.1c. These concentric lamellae are found inside osteons. Figure 1.1c shows how the osteons are built. The function of the osteoclast, shown in the figure, is to remove the bone matrix. By doing so, the bone can constantly get maintained and repaired when needed. The center of the osteons have a canal. This is known as the haversian canal, which allows blood vessel and nerves to travel through the osteons. Figure 1.2 shows a summarizing of the bone remodeling process.

To summarize, the bone is made up of cells and extracellular matrix (ECM). The ECM is made up of the organic matrix, which contains proteoglycans, glycosamino-

glycans, glycoproteins, osteonectin and collagen. It is also made up of collagen fibers and water [5]. The ECM is what glues together the cells and organs of multicellular organisms, in addition to providing a stable framework for the tissues. The framework will maintain the shapes of the bone under physical loads [6]. This function is important in order to shield embedded cells from adverse effects [7]. Not only is the ECM an important factor for maintaining shapes and withstanding stresses, it is also acting as an instructive environment for the adhesion, growth and differentiation of the cells [8].

1.2.2 Osseointegration

Osseointegration was accidentally discovered by Per-Ingvar Brånemark in 1952 [9]. His intention was to put optical devices encased in titanium into the legs of rabbits to study the blood flow. When they were going to remove the devices, they discovered that the titanium could not be removed as it had been fused into the bone. Brånemark called the process *osseointegration* [9]. The first implant in a human was a dental implant in 1965 [10]. In 1980 began the first use of osseointegration for fixating a broken bone. The broken bone was fixated together with screws and plates.

The most critical component of a separate prosthesis is the socket. The socket is the part that attaches the prosthesis to the body. This must be well fit in order to provide comfort and function. If the socket does not fit correctly, it can be painful and the mobility may be compromised. Since osseointegration is a direct structural and functional connection between the living bone tissue and the implant, one can get rid of the socket of the prosthesis. If the implant is well-designed, osseointegration can be achieved by forming an interlock on the surface of the implant with the surrounding bone

When an implant is inserted into the bone, remodeling of the bone is necessary to achieve complete osseointegration. An ideal bone graft can be divided into three stages [11]. The first step is where the protein adsorbs onto the surface of the implant. When the implant is inserted into the bone, blood vessels are torn, and fills the surrounding area with blood. The proteins from the blood, such as albumin, fibrinogen and fibronectin, adhere to the surface of the implant. This step is essential to assure the adhesion of the osteoprogenitor cells, also known as mesenchymal stem cells. The second step is when the cells adhere to the implant surface. Once the osteoprogenitor cells have adhered to the implant, the osteoprogenitor cells proliferate, meaning that the cells reproduces rapidly. The third step is where the osteoprogenitor cells differentiate into osteoblasts and forms the

organic matrix of bone.

1.2.3 The Bone Marrow

The bone marrow fills the cavities in the center of some bones. It consists of soft and spongy tissue, and can be divided into two types, red and yellow bone marrow. The bone marrow contains two types of stem cells, mesenchymal and hematopoietic. These are immature cells that each can give rise to an array of different cell types.

The hematopoietic cells can differentiate into blood cells, and are found in the red bone marrow (also known as myeloid tissue). Most of the white blood cells, all red blood cells and platelets, derives from hematopoietic cells. The white blood cells are necessary for a healthy immune system. In adulthood, the red bone marrow is composed of 40% fat, 40% water and 20% protein.

The yellow bone marrow, also known as fatty tissue, helps maintain the correct environment for the bone to function, and acts mainly as a storage of fats. Yellow bone marrow for adults is composed of 80% fat, 15% water and 5% protein [12]. The yellow bone marrow is usually located in the central cavities of long bones.

1.2.4 Bone marrow-derived Mesenchymal Stromal Cells

Cell and gene therapies with adult stem cells have gained a lot of interest over the last 40 years [13]. One of the much used stem cells is the Mesenchymal Stromal Cell (MSC). MSCs were discovered by Friedenstein when he showed that MSCs could differentiate to bone *in vitro*. He also showed that a subset of the cells had a high proliferative potential when plated at low density in tissue culture. These cells are labeled MSCs due to their function *in vitro*. MSCs can be isolated from a variety of different tissue sources. Amongst them are adipose tissue (or body fat) [14], umbilical cord [15] and bone marrow.

MSCs are being used for several applications, either therapeutic or cell-based bone tissue engineering. Table 1.1 shows different types of diseases that can be treated therapeutically by MSCs.

The bone marrow-derived mesenchymal stromal cells (BMSC) are derived from the adherent cell fraction in the bone marrow of the iliac crest. These cells are osteoprogenitor cells that have multipotent differentiation capacity *in vitro*, giving the cells the origin to osteoblasts. Due to this, the cells are often used in regenerative and tissue engineering.

Table 1.1: Therapeutic applications of MSCs on different diseases. *The different phases indicate the stages of the clinical trials. Phase I is small trials, and only recruit a few patients. The trial may be open to people with any type of cancer or disease. Phase II are larger trials, and are often compared with a placebo.

Disease	Characterization	Phase*	Outcome	References
Graft-versus-host disease (GvHD)	Rejection of host tissue by transplanted bone marrow. Can lead to inflammations in the liver, skin, and gastrointestinal tract. GvHD is a complication after bone marrow transplantation.	II	In 2008, 55 patients were infused with expanded BMSC. Thirty patients showed complete response, 9 patients showed partial response and 16 showed stable or progressive disease.	[16, 17]
Osteogenesis Imperfecta (OI)	OI is characterized by skeletal deformities and propensity for fractures. It is an inherited disorder.	I	Patients who originally recieved allogeneic bone,marrow transplants, underwent intravenous treatment with cultured BMSC 18-34 months after transplant. Five of six patients experienced improvement in growth velocity.	[18, 19]
Autism Spectrum Disorder (ASD)	ASD is characterized by difficulties with communication and interaction with other people, and restricted interests and repetitive behavior. People with ASD may also not function properly in school, work and other areas of life.	II	Treatment with MSC showed efficacy. Improvements were observed in visual, emotional, and intellectual responses. A 14-year old boy with severe ASD was treated. Improvements were found within 1 week, with eye contact and attention, fine motor activities. After 6 to 12 months the patient showed improvement in social interactions and emotions, impulse control, reading skills and hyperactivity.	[20, 21]
Multiple Sclerosis (MS)	MS is characterized by being a chronic and unpredictable disease of the central nervous system. The disease can cause many symptoms, including blurred vision, loss of balance, poor coordination and slurred speech.	II	10 patients recieved intravenous dose. A significant improvement of the visual activity and, visual evoked potentials was found, as well as an increased optic nerve area.	[22, 23]

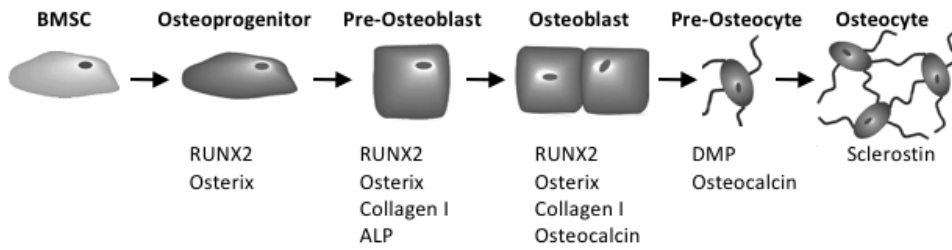


Figure 1.3: Gene expressions during osteoblast-to-osteocyte ontogeny

The figure shows the specific gene expression during the different stages of osteoblast differentiation.

1.2.5 Tissue Engineering

Tissue engineering includes research in the fields of biomaterials, cells, biomolecules, engineering design and biomechanical design. A biomaterial is a material that can be used for implants. The biomaterial should be designed to host specific cell types for certain tissues. For a biomaterial to be functional, the structures and shapes must be engineered for implantation and interaction with host tissue. The cellular response is influenced by both biomolecules and biomechanical properties[24]. This response may be characterized by using tools in e.g. gene expression and protein sequence analysis. A tissue engineered scaffold is designed to mimic the physical and biological environment surrounding a cell population.

Cells, in their natural environment, attaches to proteins in the ECM. When materials get implanted into the human body, the surface immediately gets coated with proteins from the blood. Through the layer of proteins, the cells sense the foreign surface. It is therefore the adsorbed proteins that the cells initially respond to, and not the surface of the implant [25].

Before bone tissue engineering can be applied in clinical studies, preclinical studies are performed to resemble the actual clinical situation. This research is typically performed *in vitro*. The next phase after *in vitro* research is proof of concept in animals.

1.2.6 Gene Expressions

As previously explained, osteoblastogenesis can be characterized by several phases: differentiation of MSC, mineralization of ECM, and establishment of osteocytes. These stages can be characterized by expressed genes. Figure 1.3 shows when it is expected that the gene expressions are present.

Collagen type I is the most dominant collagen in the bone, and it accounts for approximately 90% of the entire collagen content, and 80% of the total proteins in the bone [26]. Collagen serves as the template for matrix deposition and mineralization in the bone, and is therefore the main source of mechanical strength in connective tissue [27]. The collagen type I protein can be encoded by the *COL1A1* gene. *Osteocalcin* is synthesized only by osteoblasts, and is the most abundant non-collagenous protein of the bone extracellular matrix [28]. It is considered a marker of osteoblast differentiation, and has been widely used in clinical investigations, as a marker of bone formation [29]. Osteocalcin is encoded by the *BGLAP* gene.

The differentiation of osteoblasts can be characterized by the gene expressions of the Runt domain-containing transcription factor and Osterix (*SP7*).

Runt domain-containing transcription factor (RUNX2) provides instructions for making the RUNX2 protein that is involved in maintenance and development of bones, teeth, and cartilage. This protein is necessary for osteoblast differentiation, and it controls bone lineage cells by binding to the RUNX regulatory element in promoters of osteoblastogenic genes [30]. During the subsequent stages of osteoblast differentiation, the levels of the *RUNX2* gene gradually increases. *RUNX2* has a maximum expression in mature osteoblasts [31]. The *osterix* protein is a bone specific transcription factor, and is required for osteoblast differentiation and bone formation. Osterix is encoded by the *SP7* gene, and it have similar expressions to *RUNX2*. It is therefore expected to show a signal at both pre-osteoblasts and mature osteoblasts.

High levels of sclerostin, the protein product of *SOST*, indicate mature osteocytes [32]. The main function of sclerostin is to inhibit bone formation. This is to ensure that bones are of the correct shape, size and density. Sclerostin also promotes self-destruction of bone cells. A lack of sclerostin can give an overgrowth of bone due to increased bone formation [33].

1.2.7 Biomedical Challenges

One of the main challenges with implants, is the adaption of their mechanical and biomedical properties to those of natural bones. The elastic modulus of bone varies from 0.76 GPa to 34 GPa [1, 2], depending on bone density and age. In human cortical bone, the tensile and compression strengths and elastic modulus decrease approximately 2% per decade after age 20 [34]. The medical grade Ti-6Al-4V, however, has a modulus of 110 GPa. Stress shielding may occur due to the massive difference of elastic modulus from the implant and the human bone.

Stress shielding is when the mechanical load is transferred away from the adjacent bone. The absence of mechanical loading leads to a reduction in the shielded bone mass and density, and subsequently a loss of bone [35]. Due to this the current biomaterials need to have material properties such as long fatigue life combined with low elastic modulus.

Other main challenges are pain, infections and wear. Even a relatively small amount of wear can lead to significant degradation of function for some implants. It can, for example, result in a biological process known as osteolysis, which may lead to loosening of the prosthesis [4]. Since there are young patient receiving the implants, the required lifespan for the implant must be increased.

1.3 Mechanical Background

1.3.1 Additive Manufacturing

Additive Manufacturing (AM) is a formalized term for what used to be called rapid prototyping, and popularly known as 3D printing. The development of AM technology began in the early 1980s, when Chuck Hull applied for a patent of fabricating a 3D object by selectively adding material layer by layer. With AM, industries have the possibility to rapidly create a part representation before final release or commercialization. With the advancement of the technology, AM is now used to fabricate end-use products in aircrafts, automobiles, dental restorations, medical implants and others. While other manufacturing processes require a careful and detailed analysis of the part geometry and also require multiple stages to be carried out, AM technology significantly simplifies the process of producing complex 3D objects directly from the Computer Aided Design (CAD) data, into a single step.

There are various AM processes and machines that have been developed since it was first introduced in the early eighties. The most relevant AM technologies of metals commonly uses powder or wire as a feedstock, which is selectively melted by a focused heat source. Directed Energy Deposition (DED) is one of the AM processes that uses wire as feedstock. This has been described by ASTM Standard as an *"additive manufacturing process in which focused thermal energy is used to fuse materials by melting as they are being deposited"* [36]. In other words, the material is deposited by a nozzle, and then melted by a laser or electron beam.

Powder Bed Fusion (PBF) is an AM process that uses powder as feedstock. This is described by ASTM Standard as an *"additive manufacturing process in which thermal energy selectively fuses regions of a powder bed"* [36]. The PBF processes were one of the earliest invented AM processes. In order to induce fusion between powder particles, every PBF process must include one or more thermal sources. The different PBF processes must also include a method for controlling powder fusion to a prescribed region of each layer, and mechanisms for adding and smoothing powder layers. Selective Laser Melting (SLM) and Electron Beam Melting (EBM) are examples of powder bed-based processes.

1.3.2 Selective Laser Melting

Selective laser melting (SLM) emerged in the late 1980s and 1990s. The SLM process uses a laser beam to selectively melting successive layers of powder. By ap-

plying sufficient power, the powder material is heated and melted to form a liquid pool. The liquid pool is quickly solidified and cooled down. After a cross section is scanned by the laser, the building platform is lowered by an amount equal to the layer thickness, and a new layer of powder is deposited. This process is repeated until the product is completed.

Medical and dental applications are often made using SLM. This is due to their complex geometry, strong individualization and high-aggregate price. To meet the strict material requirements for additive manufactured implants regarding mechanical and chemical properties, the SLM process must guarantee high accuracy and appropriate surface roughness.

All though the SLM process have many positive features, the process also have some frequently observed problems. SLM is characterized by high temperature gradients. This results in a rapid solidification and build-up of thermal stresses. This again gives rise to the presence of non-equilibrium phases and the occurrence of segregation phenomena [37].

1.3.3 Electron Beam Melting

Electron beam melting (EBM) uses a high-energy electron beam to induce fusion between metal powder particles. The process was commercialized by Arcam AB in Sweden in 2001, and was developed at Chalmers University of Technology. The process works by heating the powder by transferring kinetic energy from incoming electrons into powder particles. Each thin layer of pre-laid powder is scanned by a focused electron beam, causing localized melting and resolidification per the slice cross section.

When an electron beam is passing through a gas at atmospheric pressure, the electrons will interact with the atom in the gas and get deflected. Therefore the process must be conducted in a vacuum state. The vacuum system provides a base pressure of 5×10^{-5} mbar or better throughout the build cycle [38]. This provides oxygen free environment and reduces the risk of hydrogen pick up, enabling accurate directionality of the beam and high purity [39]. In addition to providing an oxygen free environment, the vacuum state can allow the use of high temperatures [40]. To maintain the chemical specification of the built material, helium is introduced to 2×10^{-3} mbar during the melting process.

Since electrons have a negative charge and are focused and deflected magnetically, then the powder bed must be conductive. Due to this EBM can only be used to process conductive materials.

1.3.4 PBF Powder Characteristics and Production

Different powder production methods result in different powder characteristics. Characteristics that are important for AM are particle morphology, chemical composition and particle size. Typical production methods are water, gas and plasma atomization. For Ti and Ti alloys, electrolytic methods, metalothermic processes and hydride-dehydride process are used [41]. Water atomization is not suitable for reactive materials such as Ti.

Undesired effects of produced metal powder in AM are the oxygen uptake and the formation of oxide layers. This will impact the melt pool and influence the powder flow behaviour. Since the EBM process is conducted in a vacuum state, the environment is oxygen free, giving EBM an advantage.

1.3.5 Additive Manufacturing Challenges

There are many challenges that are considerable when printing with powder bed fusion. The powder handling is a very important aspect. The powder delivery system must transport the correct volume of powder from the powder reservoir to the build platform without any wasteful excess material. It is also important that the powder spreading does not create excessive shear forces that will disturb the previously processed layers.

With smaller powder particle sizes it is possible to achieve better surface finish, higher accuracy and thinner layers. However, small particles do have a tendency to become airborne. Airborne particles tend to settle on surrounding surfaces. This may reduce the sensitivity of sensors, deflect laser beams and damage moving parts [42].

It is difficult to predict the quality of AM components. This is because the geometry, dimensions, material characteristics and mechanical properties are all impacted by AM process. In addition, an identical component may have different quality when built using different AM machines. The microstructure can also vary due to the different cooling time of thicker and thinner sections.

1.3.6 Biomaterials

When working with biomedical materials there are many things to consider. Biomaterials must have special properties to meet the needs of a particular application. A biomaterial must be corrosion resistant, non-carcinogenic, biocompatible, low toxicity and wear resistant.

A biomaterial can be divided into three main types of biomaterials; biotolerant, bioactive and bioinert. Biotolerant materials are not rejected, but surrounded by a fibrous layer in the form of a capsule [43]. Examples of biotolerant materials are silicone gel, used for breast implants, and glass [44, 45]. Bioactive materials are characterized by establishing chemical bonds with bone tissue [46]. Examples of bioactive materials are ceramics, such as calcium pyrophosphate, tricalcium phosphate and hydroxyapatite [43, 47]. Bioinert materials have direct contact with adjacent bone tissue, and do not release any harmful substances. Examples of bioinert materials are titanium, stainless steel and cobalt-chromium [46, 48]. All three types are biocompatible, and result in a predictable host response application. These materials are all currently being utilized as structural materials in artificial hip joints, bone plates and screws and artificial dental roots.

1.3.7 Titanium-Based Alloys

Titanium, either commercially pure, or certain alloys, is, as previously mentioned, characterized as bioinert material [49]. Bioinert materials do not release any harmful substances, therefore titanium will not give any adverse tissue reactions.

As mentioned in subsection 1.2.2, Osseointegration, titanium and titanium-based alloys are widely used for osseointegration. Titanium interacts with biologic fluids through its stable oxide layer, which forms the basis for its exceptional biocompatibility [50]. Pure titanium, Ti, is body-centered cubic (BCC) at temperatures above 883°C, and hexagonal close-packed (HCP) at lower temperatures. Ti-based metals do not only integrate with the bone tissue, they also have excellent in vivo corrosion resistance. However, Ti and its alloys have a major disadvantage with a very poor wear resistance. In order to make Ti-alloys suitable for load-bearing articulating surfaces, surface modification is often needed to give greater wear resistance [4]. This can be achieved either through ion implantation or TiN film application. Commercial Purity (CP) titanium usually contains small amounts of interstitial elements, including O, N and H. Even though the quantities of these interstitial elements are small, they still affect the mechanical properties through interstitial solid strengthening. The element limits and mechanical properties for CP Ti can be seen in table 1.2.

Table 1.2: Element limits and mechanical properties for CP Ti

CP Ti is divided into four grades where grade one has the lowest O content and yield strength, and grade four has the highest O content and yield strength [4].

Grade	O_{max}	N_{max}	H_{max}	σ_{yield} (MPa)	σ_{uts} (MPa)	$\%_{elong}$
1	0.18	0.03	0.015	170	240	24
2	0.25	0.03	0.015	275	345	20
3	0.35	0.05	0.015	380	450	18
4	0.40	0.05	0.015	483	550	15

To achieve a higher yield- and fatigue strength while still maintaining the corrosion resistance and osseointegration tendency, Ti is alloyed to form a two-phase alloy, $\alpha + \beta$. These two-phased alloys are used for major load-bearing applications, while also behaving well in clinical use. The microstructure of these alloys have a superior fatigue crack initiation resistance and excellent high cycle fatigue strength. To achieve this microstructure, the alloy is treated with mill-annealing. This results in formation of small equiaxed α grains surrounded by β -phase particles. Table 1.3 shows the different mechanical properties of $\alpha + \beta$ Ti alloys.

Table 1.3: Mechanical properties of $\alpha - \beta$ Ti-alloys [4].

Alloy	E (GPa)	σ_{yield} (MPa)	σ_{uts} (MPa)	$\%_{elong}$	$\sigma_f(10^7)$
Ti-6Al-4V	110	860	930	10-15	610-625
Ti-6Al-7Nb	105	795	860	10	500-600
Ti-5Al-2.5Fe	110	820	900	6	580

The most commonly used titanium alloy is Ti-6Al-4V, and accounts for more than 60% of the titanium alloy production [51]. The alloy belongs to the $\alpha + \beta$ -group, and have a high tensile strength, with good fatigue and fracture properties. It is used in many products, such as aerospace industry, marine applications, chemical industry, gas turbines and biomechanical applications [52]. This is mostly due to it's high ultimate and yield strength, but it is also due to it's capability to be manufactured using AM. However, due to Ti-6Al-4V's poor shear strength, it is undesirable for bone screws or plates. It also tends to seize when in sliding contact with itself and other metals. This is due to it's poor surface wear properties.

1.3.8 Additive Manufactured Ti-6Al-4V

Ti-6Al-4V can be manufactured using several AM processes, including DED, with both laser and electron metal wire deposition, and PBF processes, with SLM and EBM. The US Food and Drug Administration (FDA) have previously approved Ti-6Al-4V implantable devices manufactured with EBM [53]. The quality, such as overall dimensions, feature geometry, material characteristics and mechanical properties, are impacted by AM. An identical component may have different quality when built using different AM machines.

Previous research have shown that EBM Ti-6Al-4V is composed of α lamellas, and a small amount of β phase [54, 55]. Thinner sections, with a thickness of 500 μm -1000 μm , have alternate α/β mixed with acicular α' martensite [56]. The martensitic phase is likely formed due to a fast solidification of the melt pool for the thinner sections. The thickness of the lamellas decreases with the part size, this is also likely a result of the faster cooling rate of the smaller specimens. The decreased thickness of the α lamellas mixed with acicular α' martensite result in an improvement in strength and decrease in ductility.

All though EBM is said to be free of oxygen, EBM manufactured Ti-6Al-4V is still protected with an oxide layer. This oxide layer likely occurs during the EBM process. When the powder is preheated with the electron beam, the temperatures increases, and water molecules are released and become available for reaction with the titanium surface [57]. This oxide layer protect the underlying metal from further reactions, such as corrosion [58]. It has also been suggested that the oxide layers have significant influence on the integration of the metal with human bone [59, 60].

Most studies reveal that AM Ti-6Al-4V have better mechanical properties than the conventionally fabricated titanium alloys [61]. See table 1.4 for a comparison of EBM and SLM fabricated Ti6Al4V, compared to wrought and cast material.

Table 1.4: Comparison of EBM, SLM, wrought and cast fabricated Ti-6Al-4V

Mechanical properties of EBM manufactured Ti-6Al-4V compared to wrought and cast material [52]. *ASTM F1108 (cast material) **ASTM F1472 (wrought material)

	EBM [52]	SLM [54]	Ti-6Al-4V*	Ti-6Al-4V**
YS (Rp 0.2)	950 MPa	1200 MPa	758 MPa	860 MPa
UTS (Rm)	1020 MPa	1310 MPa	860 MPa	930 MPa
Elongation	20%	22%	>8%	>10%
Area reduction	50%	50%	>14%	>25%
E-Modulus	110 GPa			

2 | Aim of Thesis

The scope of this thesis has been to design and manufacture a porous scaffold, and to understand the effects of the biocompatibility and osteogenic properties of these. This was studied by conducting *in vitro* experiments of the designed scaffolds. These experiments made it possible to discover the adhesion, proliferation and differentiation capacity of BMSCs cultured on scaffolds. If the scaffold is not biocompatible, the implant will not be able to live in harmony with the body, and the body will reject it. The osteogenic properties determine the osseointegration between the bone and the implant.

Figure 2.1 gives an explanation of what will affect the mechanical properties and osteogenesis of the implant. By using a solid implant, there is no need for AM to manufacture the implant, and therefore AM will not affect the mechanical properties. However, when a porous scaffold is manufactured, it is not possible to do this without the use of AM. In short, the scaffold's geometry and manufacturing process will affect both the mechanical properties and the osteogenesis.

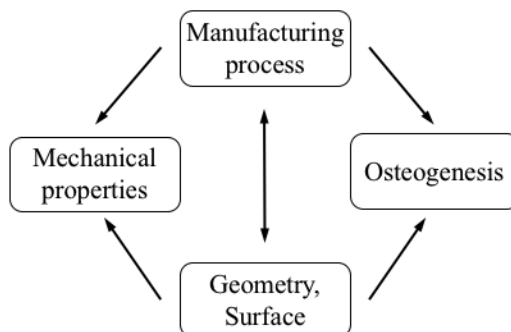


Figure 2.1: The processes that affects the osteogenesis and mechanical properties

The figure shows an explanation of what affects the osteogenesis and mechanical properties.

The mechanical properties are very important in achieving a long lasting implant. The implant should, as previously mentioned, have a Young's modulus similar to human bone (*i.e.* 0,2-34 GPa [1, 2]), in addition to a long fatigue life. When changing the surface roughness, lattice structure and pore size, the mechanical properties will also change. Therefore it makes sense to find the optimal geometry and surface in regard to the biocompatibility of the scaffold, before investigating its mechanical properties.

Specifically, the aim of this thesis can be described in parts as:

- Design and manufacture porous scaffolds. The scaffolds will be manufactured using AM, with the alloy Ti-6Al-4V, grade 5.
- Discover the biocompatibility of the scaffolds by seeding the scaffolds with BMSCs to see how the cells react to the scaffolds. If the cells adhere to the surface and subsequently proliferate, then the scaffolds have a biocompatibility which is expected for the Ti-6Al-4V alloy.
- Investigate the osteogenic properties of scaffolds by finding the differentiation capacity of the BMSCs when seeded on the scaffolds. This will be studied by using different assays and methods, such as ALP staining, Alizarin Red staining and PCR analysis.

2.1 Research Background and Motivation

The first thing that intrigued me by this project was to get the opportunity to discover the mechanical properties of additive manufactured components. I have for a long time been very fascinated by the additive manufacturing world, and this was an opportunity I did not want to miss. However, when I started to work on this project, I was introduced to the actual topic of this project; additive manufactured *implants*. This was a whole new world for me. The fact that titanium could form a proper interlocking with human bone made this project even more interesting. What I later was to discover, was that many friends, acquaintances and family members had implants. From hearing their personal experiences, I have seen how important this field is. This is what motivated and interested me in this research field.

Before I started working on this thesis, I only had a background within the mechanical engineering field, with a deeper focus in product development and materials engineering. After I was introduced to this topic, I had to learn biomed-

ical theory and techniques, in order to perform the experimental methods and to analyze the results.

Throughout this thesis I have learned the theoretical background of bone structure and bone remodeling. I have learned how to do cell culturing, use assays to assess different results, in addition to independent use of several equipments, such as fluorescence microscopy, PCR equipment and many other. I am very grateful for getting the opportunity to learn about both tissue engineering, and the necessary techniques behind it.

All though additive manufacturing was not an unfamiliar topic for me, I still had to dig deep into previous literature and theory, in order to interpret the theory behind additive manufactured scaffolds.

2.2 Outline

In search of a biocompatible scaffold with a high osteogenic property, the adhesion, proliferation and differentiation capacity of BMSCs cultured on titanium scaffolds was analyzed.

The previous chapter, **Chapter 1**, will give the reader a basic understanding of the theory behind the research done in this thesis.

In **Chapter 3**, the experimental methods used was described. This chapter include the description of certain cell culturing methods, which was necessary prior to the actual experiments. Next, the chapter describes how the metabolic activity was found by using the alamarBlue[®] assay. The staining protocol for the ALP activity was described, in addition to the ARS staining method, which was performed in order to stain the calcium deposition. Finally the method for the PCR analysis was described.

Chapter 4 presents the results and knowledge gained from the experimental work, and the highlights of the results were commented on.

Chapter 5 gives an analyzing and discussion of the presented results. The focus of the discussion was to evaluate if the scaffolds were biocompatible in addition to having high osteogenic properties. The challenges that occurred during the experimental method was also assessed.

Chapter 6 presents a summarize and a final conclusion of the discussed results. Finally, **Chapter 7**, presents the future research plans within this topic.

2.3 State of the Art

This section will introduce previous research in this field. The section will mostly focus on the osteogenic properties of scaffolds with different pore size and porosities.

2.3.1 Effects of Pore Size and Porosity, *in vivo*

It is still controversial in literature on which pore size and porosity enhances osteogenesis. Hulbert et al. [62] discovered bone tissue ingrowth when the pore size was greater than 100 μm . When the pore size was greater than 150 μm , they discovered initiation of osteogenesis. It was also claimed that larger pore size allowed greater number of blood vessels to grow into [62]. Feng Bai et al. [63] implanted β -tricalcium phosphate (β -TCP) *in vivo* in a rabbit, and discovered that there was no improvement in vascularization in scaffolds with pore size above 400 μm , indicating the upper limit of pore size for vascularization is 400 μm .

Naoya Taniguchi et al. [64] manufactured implants of CP Ti using SLM with three different pore sizes, 300 μm , 600 μm and 900 μm , with the intended porosity of 65 %, and did *in vivo* testing of these in rabbits. The results showed higher fixation for 600 μm than for 300 and 900 μm . The scaffold with pore size 300 μm showed an inferior bone ingrowth compared to 600 and 900 μm . Johan Van der Stok et al. [65] also used SLM to manufacture scaffolds with pore sizes of 120 μm and 230 μm with two different porosities; 88% and 68%, and implanted these in Wistar rats. The result showed that the porous scaffolds did facilitate bone formation an equal amount on both the scaffolds.

Su-Hua Wu et al. [66] used EBM to manufacture Ti-6Al-4V porous scaffolds, with pore size $710 \pm 42 \mu\text{m}$ and porosity 68 %, and did a spinal fusion of these in a sheep. This resulted in a fast bone ingrowth, and promoted a good osseointegration.

2.3.2 Effects of Pore Size and Porosity, *in vitro*

Timothy Jørholm has previously investigated the differentiation and bone deposition of BMSC on AM porous Ti-6Al-4V scaffolds during his Master's thesis. All the results given in this section have been retrieved from his thesis (*Differentiation and Bone Deposition of Bone Marrow Derived Stem Cells on Additive Manufactured Porous Ti-6Al-4V Scaffolds*, June 2017, NTNU, Timothy Jørholm) [67].

When Jørholm designed the scaffolds, he modeled the parts in SOLIDWORKS

(DassaultSystems, France). The result was fully rounded cubic lattices, tilted at a 35° angle to optimize it for microscopy. The pore- and lattice strut diameter were set to $800\text{ }\mu\text{m}$. Two types of scaffolds were made; one designed to fit inside a 96-well plate, with a diameter of 6 mm, and the other designed to fit inside a 24-well plate, with diameter 14.6 mm. Both scaffolds had a height of 5 mm. The scaffolds were manufactured by an AM group (FIT AG, Lupburg, Germany), using EBM technology.

2.3.2.1 Mechanical Characteristics

The resulting scaffold had a surface roughness close to $\sim 50\text{ }\mu\text{m}$. Figure 2.3 shows the surface characterization at 100X and 500X magnification. Figure 2.2 shows close-up images of the grains.

Jøraholmen also did a static compression test using Finite Element Analysis (FEA). This result gave a Young's modulus of 16.5 GPa. He also conducted a physical compression test. This test gave an elastic modulus of 7.9 GPa.

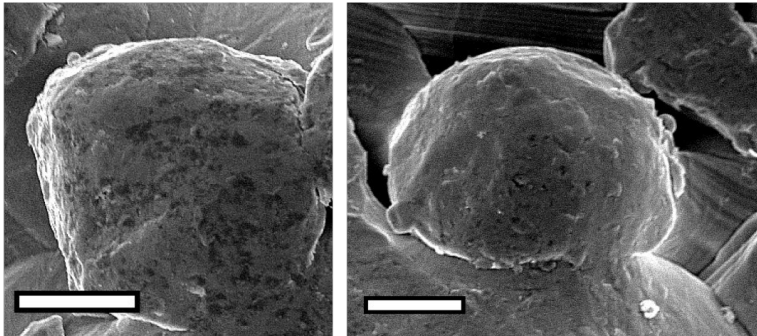


Figure 2.2: Close-up images of grains

The images show close-ups of grains. The scalebars are set to $30\text{ }\mu\text{m}$ [67].

2.3.2.2 Metabolic Activity and Adhesion

In addition to finding mechanical characteristics of the scaffolds, Jøraholmen measured cell activity using the alamarBlue® assay, figure 2.4. To see if the BMSCs adhered to the surface, he stained the cells at different set time point, and then did fluorescent microscopy to characterize cell adhesion, as shown in figure 2.5.

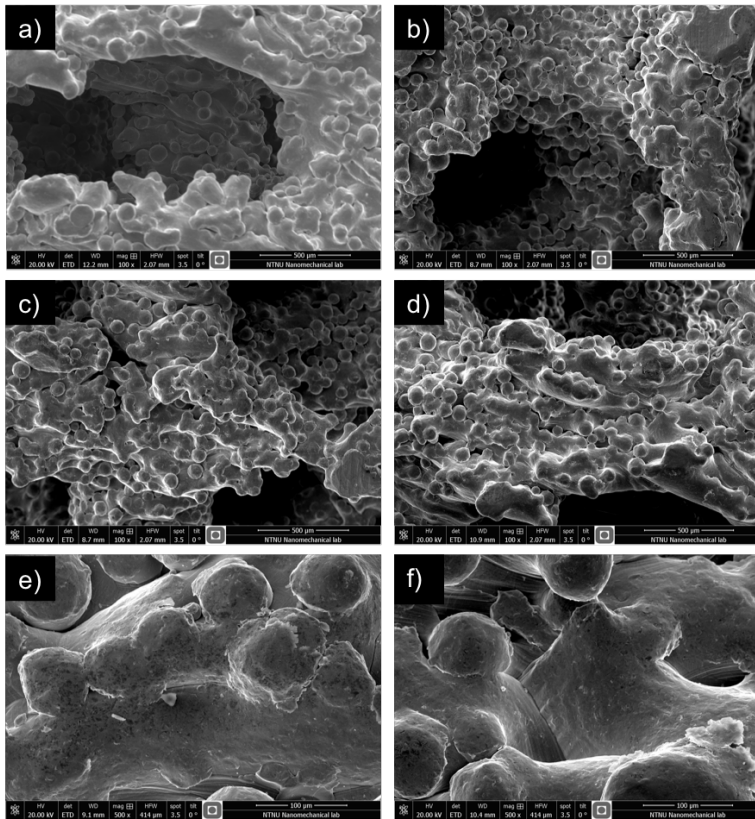


Figure 2.3: Characterization of the surface by SEM

The figure show SEM images of the surface of scaffolds. Image a) to d) are taken at 100X magnification, and e) and f) are taken at 500X magnification [67].

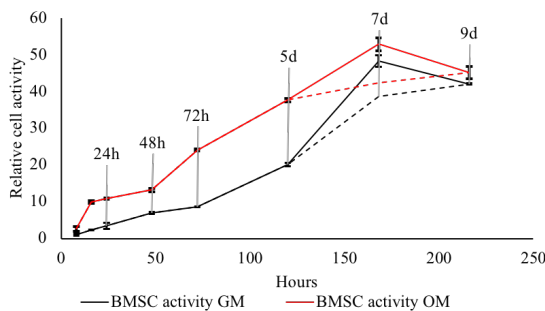


Figure 2.4: AlamarBlue® results

The graph shows the relative cell activity measured by using the assay alamarBlue®. The red graph is for the scaffold cultured with OM, and the black is for the scaffold cultured with GM [67].

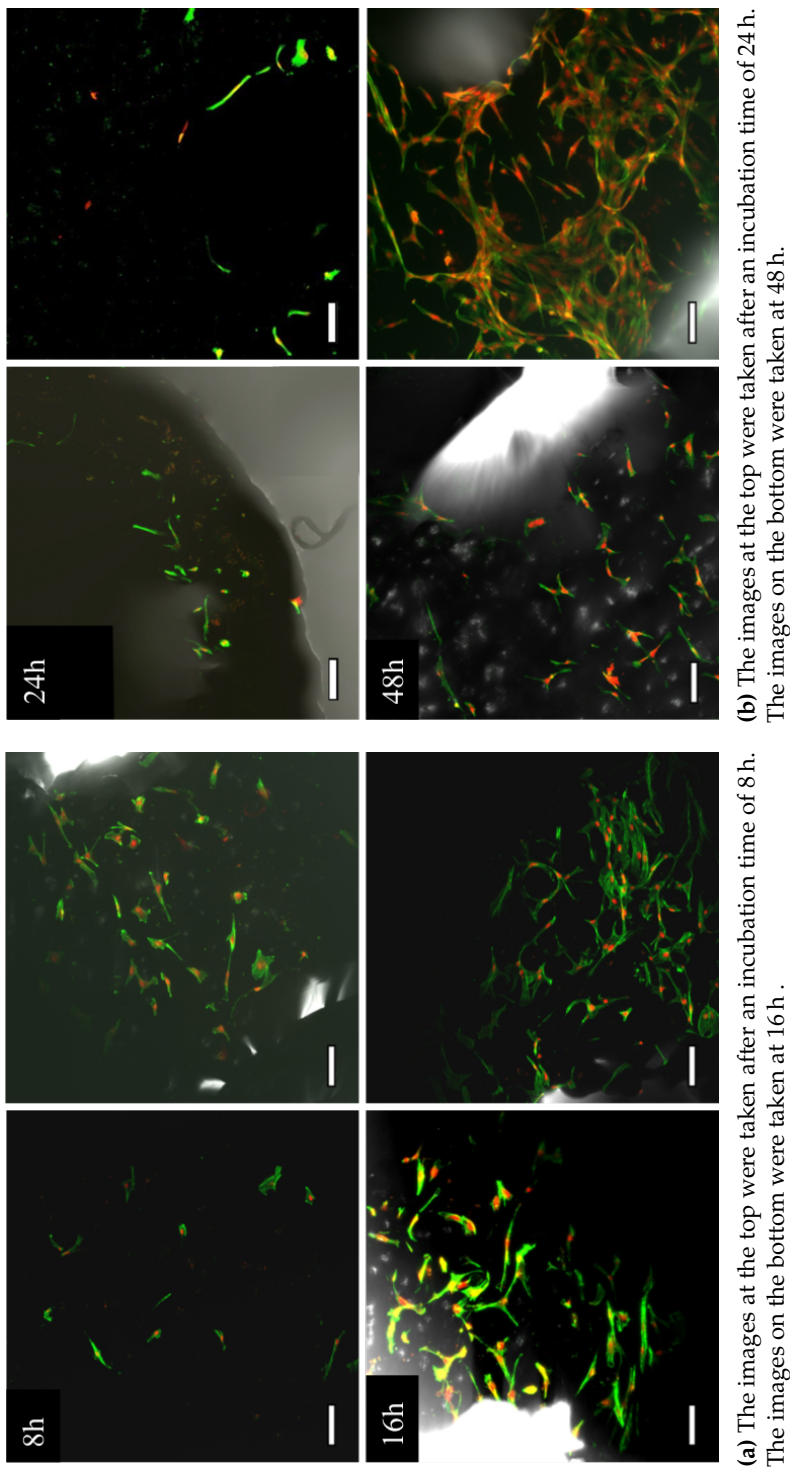


Figure 2.5: Fluorescent micrographs of the adhesion of BMSCs cultured on scaffolds
Scalebars are set to 100 µm. Alexa Fluor@488 Phalloidin (green) was used to stain the cytoskeletons, and Draq5™(red) was used to stain the nuclei [67].

2.3.2.3 Osteoblast Differentiation

To determine osteoblastogenesis, Jøraholmen performed PCR analysis to determine gene expressions of osteoblast specific genes. He conducted two separate experiments, labeled R1 and R2. The results from round 1 are normalized with respect to day 0, and results from round 2 are normalized with respect to the scaffold cultured with osteogenic medium (OM) at day 7, labeled as OM 3D D7. The plots labeled 3D, are from the 24-well scaffolds, and the plots labeled 2D are 2D blank controls, cultured in 6-well plates.

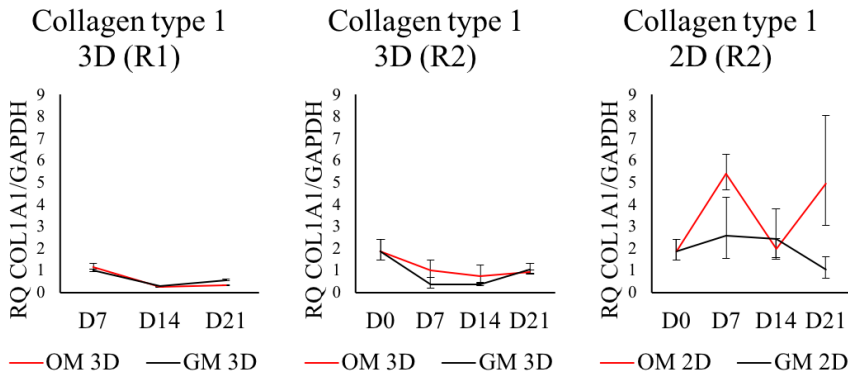


Figure 2.6: Collagen Type I expressions [67]

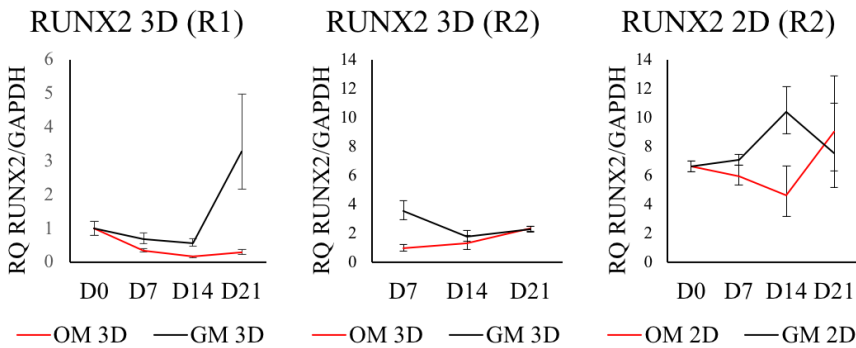


Figure 2.7: RUNX2 expressions [67]

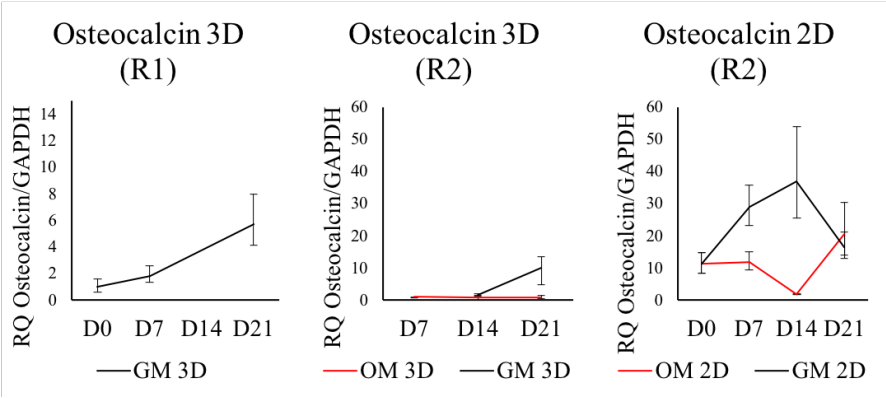


Figure 2.8: Osteocalcin expressions [67]

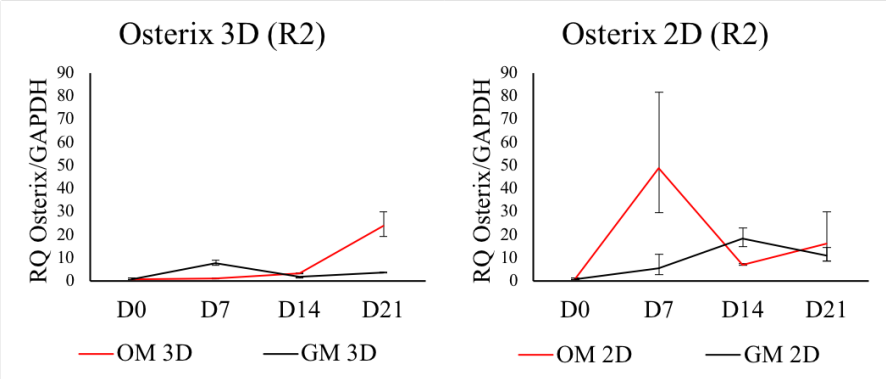


Figure 2.9: Osterix expressions [67]

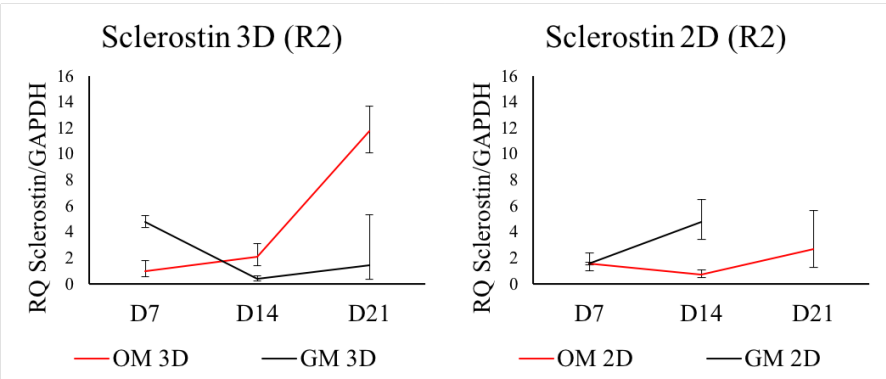


Figure 2.10: Sclerostin expressions [67]

In addition to performing PCR analysis to determine the osteoblast differentiation, Jøraholmen used ARS staining to stain the calcium deposition of mature osteoblasts. Figure 2.11a and b show the stained calcium deposition, and figure 2.11c show the relative absorbance of the calcium deposit.

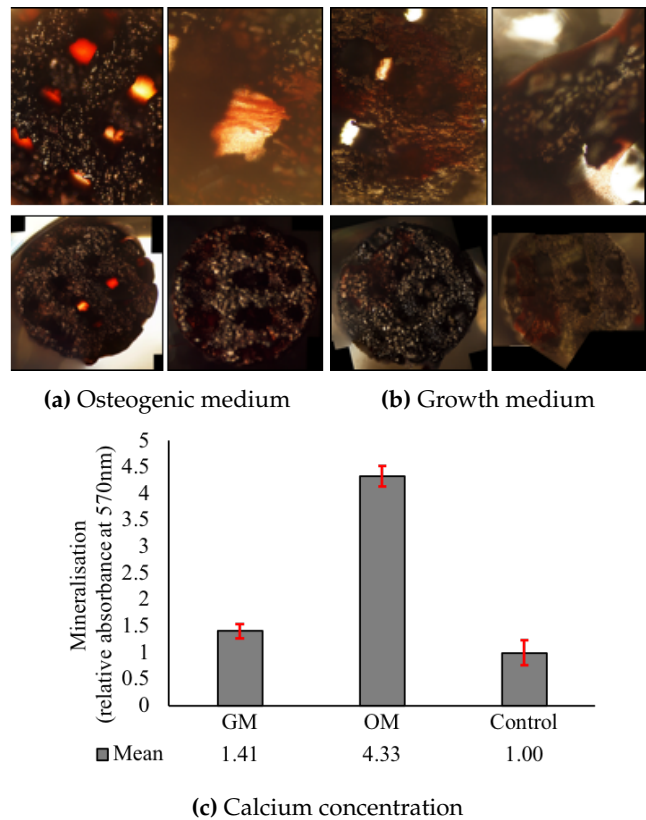


Figure 2.11: Calcium deposition

The micrographs in figure (a) and (b) show the staining of calcium deposition, by using alizarin red staining (ARS). The red color show stained calcium deposition. The micrographs in (a) show the scaffold cultured with osteogenic medium, while micrographs in (b) show the scaffold cultured with growth medium.

The graph in figure (c) shows the calcium deposition as relative adsorbance. [67]

2.3.2.4 Conclusion

Based on the results, it was concluded that porous EBM manufactured Ti-6Al-4V scaffolds, have an elastic modulus within the range of human bone.

The cells cultured on the scaffolds have clearly adhered to the surfaces, and show a good proliferation capacity. The ARS staining shows that the BMSCs have differentiated to mature osteoblasts when cultured on scaffolds. The results from the PCR analysis are, however, inconclusive.

The research performed by Timothy Jøraholmen laid the foundation for the study in this thesis. More experiments are needed in order to validate the results from the ARS staining performed by Jøraholmen. In addition, it would be beneficial to get conclusive results from the PCR analysis, to see if the desired gene expression are present in BMSCs cultured on the scaffolds, and to find the ALP activity of the BMSCs.

3 | Experimental Methods

This chapter will go through the experimental methods that was used for this study. First, the scaffold design and manufacturing will be described. Next, the experimental set up for cell culturing will be described. Finally, the techniques and methods used after cell culturing will be described.

3.1 Mechanical Methods

The mechanical methods used for this thesis will be described in this section. These mechanical methods include the scaffold design, scaffold manufacturing and porosity calculations.

3.1.1 Scaffold Design

Three types of scaffolds were manufactured, two types to fit in a 24-well plate, and one to fit in a 96-well plate. In addition, a solid 2D control, of the same material, was designed. This was designed to fit into a 6-well plate. The scaffolds were made up by many lattice structures, as shown in figure 3.1.

Figure 3.1 shows 4 lattices structures combined together. Both the lattices and the pores have a diameter of 800 μm . Figure 3.2 shows the designed scaffolds.

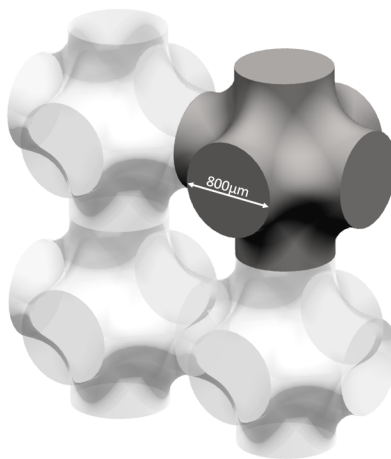


Figure 3.1: Lattice structure

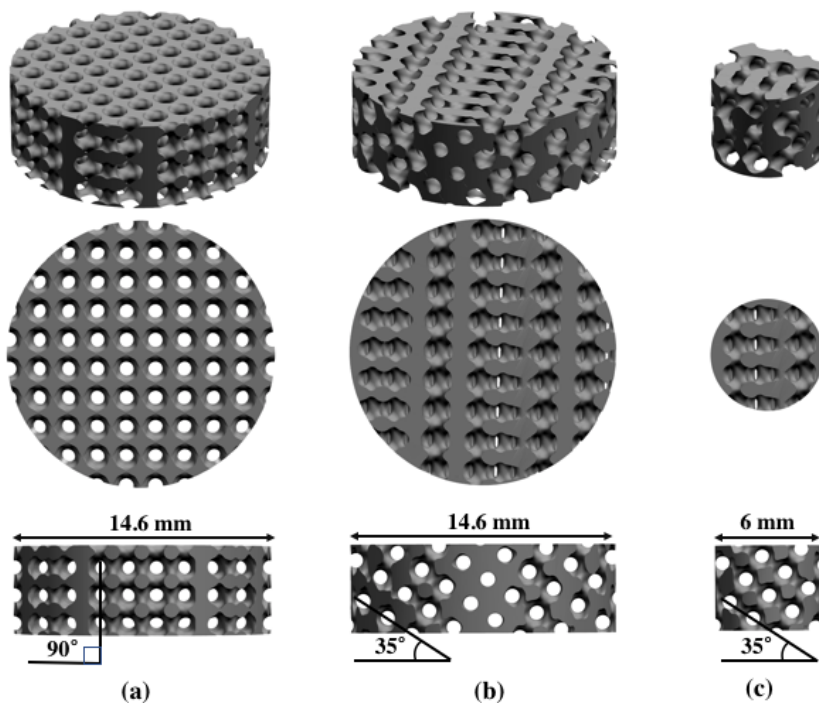


Figure 3.2: The designed scaffolds used for cell culturing
Scaffold (a) and (b) were both designed for 24 well plate. Scaffold (c) is designed for 96 well plate. Scaffolds (b) and (c) were optimized for microscopy characterization, with an angle of 35°

3.1.2 Scaffold Manufacturing

The scaffolds and controls were manufactured by the AM-group, FIT AG (Lupburg, Germany), using EBM as manufacturing process. The scaffolds were manufactured with the Ti-6Al-4V grade 5 alloy. The manufacturer have specialized in medical implantes manufactured by EBM with Ti-6Al-4V alloy. By thoroughly monitoring the manufacturing process, the manufacturer have fulfilled the European guidelines for the production of medical devices, found in the ISO 13485 standard. The process has also been approved by the US-American FDA [68]. Some of the settings used for the manufacturing process are shown in table 3.1.

Table 3.1: EBM settings

The table give some of the settings used during the manufacturing of the scaffolds. The data is provided by the manufacturer.

Setting	Value
Hatch Line offset	200 μm
Number of contours	4
Power (max, electron gun)	3000 W

The manufacturer also provided with a material data sheet for Ti-6Al-4V parts produced with EBM, as shown in table 3.2.

Table 3.2: Material data sheet for EBM manufactured Ti-6Al-4V

The table give the material properties and process-related properties provided by the manufacturer [69].

Material Properties	Value	Unit
Max. tensile strength	1020	MPa
Elastic modulus	120	GPa
Yield Strength	950	MPa
Elongation at break	14	%
Reduction of area	40	%
Hardness (Rockwell)	33	HRC
Fatigue strength (@600MPa)	>10,000,000	Cycles
Process-related properties	Value	Unit
Roughness (R_a/R_z)	15-25/80-100	μm
Achievable part accuracy	± 200	μm

In order to calculate the porosity of the scaffolds, the solid volume of the scaffolds was found using the CAD software, Siemens NX, and then the total volume was calculated. By using the total volume and the solid volume, the open pore volume can be calculated. The porosity was calculated theoretically by volumes using equation 3.1.

$$\phi_{\%} = \frac{V_p}{V_T} * 100\% \quad (3.1)$$

Where $\phi_{\%}$ is the percentage porosity, V_p is the void volume and V_T is the total volume including the voids and solids of the material.

Due to the simple geometry of the scaffolds, the porosity of the manufactured scaffolds can be determined theoretically. In order to find the density of the material, the 2D solid control was weighed using an electronic laboratory balance, and then measured. After this the scaffolds were weighed. The porosity was calculated theoretically by density and volumes using equation 3.2.

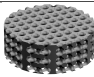



$$\phi_{\%} = \frac{m_s}{\rho_{Ti6Al4V} * V_T} \quad (3.2)$$

Where $\phi_{\%}$ is the percentage porosity, $\rho_{Ti6Al4V}$ is the measured density of the EBM manufactured Ti-6Al-4V 2D control, m_s is the mass of the scaffold, and V_T is the total volume, including voids and solids, of the scaffold.

For future referencing, the scaffolds and controls will be referred with the names given in table 3.3.

Table 3.3: Referring of scaffolds and controls

The table gives the referring names of the scaffolds and controls. The large scaffolds are designed to fit in a 24-well plate and the small scaffolds are designed to fit in a 96-well plate. The two controls, Ti and blank, are used in 6-well plates.

Image	Name	Diameter (mm)	Height (mm)	Angle (°)
	Large scaffold	14.6	5	90
	Large opti scaffold	14.6	5	35
	Small scaffold	6	5	35
	Ti control	33	2	-
	Blank control	-	-	-

3.2 Biomedical Methods

In order to assess the biocompatibility and osteogenic potential for the scaffolds, the scaffolds had to be seeded with BMSCs. The assay AlamarBlue[®] was used to determine the metabolic cell activity. Alizarin Red S (ARS) staining was used to identify calcium deposit by mature osteoblasts. Alkaline Phosphatase (ALP) staining was used to measure the ALP activity. And finally, PCR analysis was used to characterize the differentiation of the BMSCs on the scaffolds. The analysis had three set time points (0 d, 7 d, 14 d and 21 d), whereas ALP had one set time point at (10 d), and ARS staining had one set time point (21 d). Prior to seeding the scaffolds and controls with cells, they had to be sterilized by autoclaving them. This was done by a trained employee at the laboratory at St. Olavs hospital, Trondheim.

3.2.1 Experimental Setup

3.2.1.1 Cell Culturing

BMSCs were used for the cell culturing. The cells were derived from the bone marrow of a healthy, young, donor. These cells were used because they have previously shown an extensive proliferation and differentiation capacity *in vitro* and *in vivo* [13]. The cells were used before passage 07. A passage is when cells are subcultured, and trypsinized for freezing, and then thawed and reseeded. Previous research has shown that BMSCs lose their differentiation potential after the 6th passage [70, 71].

Two types of medium were needed for cell culturing. One medium to maintain the cells, labeled growth medium (GM). The second type of medium needed, is a medium designed to induce the differentiation capacity of the cells. This is labeled osteogenic medium (OM). Both mediums consists of a basic medium.

The **basic medium** consists of Minimum Essential Media Eagle (MEM- α , Thermo Fisher Scientific, Massachusetts, USA), with antibiotics (5000 IE/mL). This medium was used for both the growth medium and the osteogenic medium.

The **growth medium₁** (GM₁) is based on the basic medium with heparin (10 U/mL), glutamine (3.4 mM) and Platelet Lysate (PL)(5 %). PL was filtered using a 0.45 μ m sterile syringe filter. The growth medium₁ is used to maintain cells in the culture.

The **growth medium₂** (GM₂) is based on the basic medium with glutamine (2 mM) and Fetal Bovine Serum (FBS) (10 %). The growth medium₂ is used for the cells in culture, when cultured on the scaffolds.

The **osteogenic medium** (OM) is based on the basic medium with 2mM glutamine, vitamin C (0.2mM), dexamethasone (10^{-6} mM) and FBS (10 %). The osteogenic medium is used to induce differentiation after the scaffolds have been seeded with BMSCs. Dexamethasone, L-ascorbic acid (vitamin C) and glutamine are the essential components for differentiation in the osteogenic medium [72].

3.2.1.2 Seeding of Cells

The large scaffolds were seeded with 2×10^6 BMSCs, in 750 μ L, and the small scaffolds were seeded with 4×10^5 cells, in 150 μ L (see figure 3.3 for the reference names). This was determined by the volume ratio of the scaffolds. Both Ti and blank controls were seeded with 4×10^4 , in 2 mL.

Cryovials, containing BMSCs (donor 06, passage 6), were retrieved from the cryogenic freezer and thawed, using a water bath (37 °C). Cryovials are designed for storing biological materials at very low temperatures. However, the liquid nitrogen can, in rare occasions, leak into the vials causing the vials to explode when thawed. Due to this, the vials were thawed in a sealed thick walled container containing water (37 °C).

After thawing, the cryovials were disinfected on the outside, using ethanol. The reason for this is because liquid nitrogen is not sterile. After disinfection, GM₁ was added to the cells, and the cell suspension was spun in the centrifuge (953 g, 5 min, RT). The supernatant was poured off, and the pellet was resuspended with 1000 μ L GM₁, and then an additional amount of GM₁ was added. Next, the cells were seeded in 175 cm² culture flask, with 30 mL in each flask, and incubated (4 d, 37 °C, 5 % CO₂), until ~90 % confluent.

In order to seed the scaffolds with cells, the cells had to be trypsinized after the incubation. Trypsination will get the adherent cell to dissociate from the flask that the cells were cultured in. First, the old GM₁ in the culture flasks had to be removed, and the flasks were washed with Dulbecco's Phosphate Buffered Saline (PBS) (10 mL). The PBS was poured off, and trypsin (2.5 mL) was added to the flasks and evenly distributed. The flasks were incubated for a couple of minutes until the cells had dissociated. A microscope was used to observe when the cells had dissociated. Old GM₁ (7 mL) was added to the flask to inactivate the trypsin, and the content was poured into a tube. This was then centrifuged (953 g,

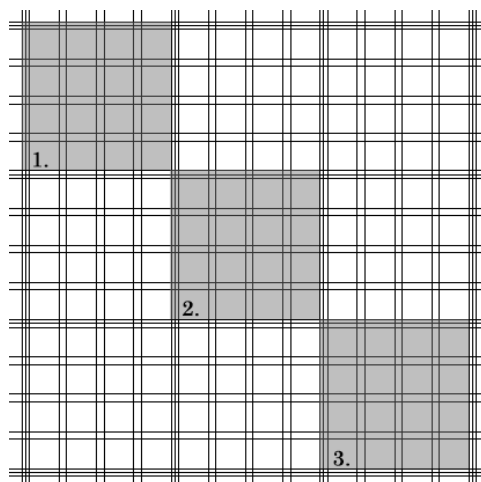


Figure 3.3: Grid pattern of a Bürker chamber

The shaded areas numbered 1, 2 and 3 indicate the counted areas. The average of the three counted areas is found, and then multiplied by 10 000 to get the amount of cells per mL.

5 min, RT), and the supernatant was poured off. Fresh medium (GM₂, without FBS, 1000 μ L) was used to resuspend the cell pellet. An additional predetermined amount of fresh medium (GM₂, without FBS) was added to the resuspended cells before the cells were counted.

3.2.1.3 Cell Counting

Principle: It is important to have an evenly distributed amount of cells on each surface. This is to get comparable results. A Bürker chamber was used to count the cells. The Bürker chamber consists of a thick glass microscopy slide and a thin coverslip. The coverslip must be properly attached to the thick glass microscopy slide. The thick glass microscope slide has a rectangular indentation that creates a chamber which is engraved with a laser-etched grid of perpendicular lines.

Experimental: The cell suspension was first thoroughly mixed using a pipette. A small amount of the suspension (10 μ L) was then pipetted to the edge of the coverslip that was attached to the thick glass slide. The Bürker chamber was placed into a microscope, and the number of cells were counted to find the cell concentration, as figure 3.3 shows. The shaded areas numbered 1, 2 and 3 were counted, and the average of these was found, and finally multiplied by 10 000 to get the amount of cells per mL.

3.2.1.4 Fixation

Principle: By fixating cells, the cell morphology and tissue architecture is preserved and stabilized. The fixation also strengthens the samples so they can withstand further processing and staining [73]. Paraformaldehyde (PFA) is one of the most used reagents for fixation [74, 75].

Experimental: The cells and scaffolds were first washed with PBS. This step was repeated 2-4 times, until the scaffolds/controls were completely clean from medium. Remaining PBS was removed from the scaffolds, before the cells were fixed with PFA (3.7 %, 15 min, RT). The scaffolds were then rinsed again with PBS four times. The fixed cells were stored cold, with PBS, until used. If the cells were stored for a long period, the cells were fixed one more time prior to usage.

3.2.2 AlamarBlue

Principle: AlamarBlue[®] is a non-toxic assay that is designed to measure the metabolic activity of human and animal cell lines, bacteria, plant and fungi. This was used in order to measure the metabolic activity of the BMSCs cultured on the Ti controls.

Experimental: Two Ti controls were seeded with BMSCs, where one was cultured with OM and the other was cultured with GM. In addition, two metal controls (MC), with cell-free medium, were used as negative controls. The metal controls were used in order to get the result of the cells, and not of the metal. The two MCs were incubated with medium, and treated exactly the same as the ones seeded with BMSCs. The controls were incubated (37 °C, 5 % CO₂). At set time points (4 h, 22 h, 46 h, 70 h, 5 d and 7 d), alamarBlue[®] (10 %) was added to the medium, and incubated (2 h, 37 °C, 5 % CO₂), before the supernatant was harvested. New medium was then added to the wells, and incubation followed until the following time point.

Once the supernatant was harvested, 150 µL was transferred to a black, solid bottom 96-well plate. Each sample was measured in triplicates. The 96-well plate was then measured in a multilabel fluorescence reader (Victor ³, PerkinElmer, Waltham, USA), using an alamarBlue[®]-dedicated analysis setup.

To calculate the relative metabolic activity, absorbance measurements of the MCs were subtracted from the results of the BMSC seeded controls. This result was then normalized with respect to the first reading (at 6 h). The standard deviation

was found by adding the standard deviation of the BMSC absorbance, with the standard deviation of the metal control, as equation 3.3 shows.

$$SD_{tot} = SD_{met.cont.} + SD_{BMSC} \quad (3.3)$$

Where SD_{tot} is the total standard deviation, $SD_{met.cont.}$ is the standard deviation of the results from the absorbance to the metal control, and SD_{BMSC} is the standard deviation of the controls cultured with BMSC.

3.2.3 Alkaline Phosphatase Assay

Principle: Alkaline Phosphatase (ALP) staining is used to detect alkaline phosphatase enzymatic activity, and is used as an early marker of osteoblastogenesis.

The *ELF®Endogenous Phosphatase Kit* is used to detect the phosphatase activity in fixed, cultured cells. The kit contains the ELF 97 phosphatase substrate and a detection buffer. When performing ALP staining, it is usually performed with multiple staining with other fluorescent dyes. Among others are Draq5™, which is a DNA stain for use in live or fixed cells. It emits in the far-red region and crosses cell and nuclear membranes in fixed cells. This was used to find the cell nucleus, and to see how much ALP activity there was, compared to nuclei.

Experimental: Small scaffolds were seeded with BMSCs and cultured with both OM and GM. Cells at day 10 were fixed as described in subsection 3.2.1.4; Fixation. After being fixed, the cells were permeabilised and blocked (0.5 % saponin, 1 % HS and PBS), and incubated (10 min, RT). The cells were subsequently rinsed with PBS (for at least 10 min). Draq5 was added to the small scaffold with a 1:1000 dilution in PBS. The Draq5 solution should cover the entire scaffold. Incubate in room temperature for 30 minutes, while preventing any exposure to light. The ELF97 dilution was prepared fresh. The optimal concentration for the small scaffolds is a 20-fold dilution series, i.e 1:20 ratio with ELF 97 phosphatase substrate (component A) and detection buffer (component B). Before the substrate solution was added to the scaffolds, the PBS was removed, and the scaffolds were transferred to a 35 mm glass bottom dish for fluorescence microscopy. The experimental methods for the fluorescence microscopy is explained in subsection 3.2.4

3.2.4 Fluorescence Microscopy

Principle: Fluorescence microscopy gives the possibility to analyse a large number of cells in a relatively short period of time by using several fluorescent probes

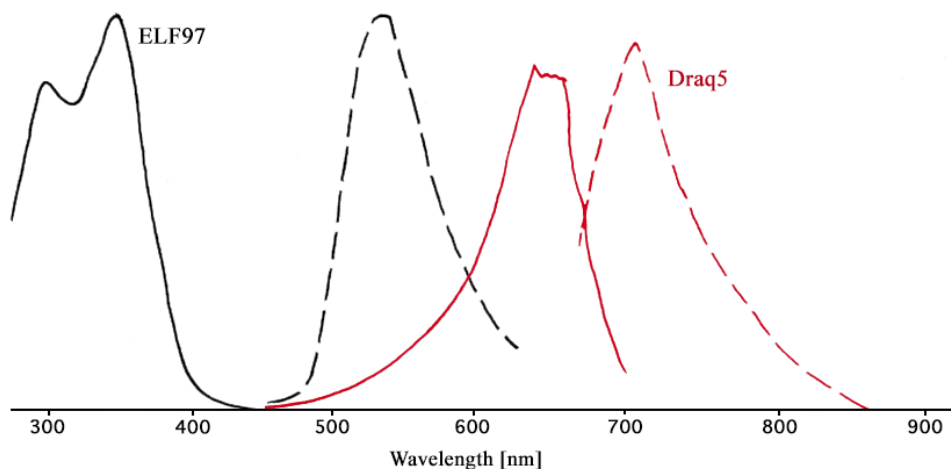


Figure 3.4: Normalized excitation and emission spectra

The normalized excitation and emission spectra of ELF 97 (black) and Draq5 (red). The excitation is marked with closed lines, and the emission is marked with dotted lines.

[76]. Compounds that exhibit fluorescence are called fluorochrome. Once a fluorochrome absorbs light, energy is taken up for the excitation of electrons to higher energy states. The process is immediately followed by lower energy states that can give emission of light. The excitation and emission take place at different regions of the light spectrum (see Figure 3.4). To get a vision of the emission, a filter is necessary. The filters are designed to pass or reject wavelengths of light [77]. A filter is either known as longpass (LP) filter or shortpass (SP) filter. LP-filter transmits light of longer wavelengths and block short wavelengths, while SP-filter transmit shorter wavelengths and block long wavelengths. When choosing a filter for the fluorescence microscopy of the staining of ELF 97 and Draq5, it is important to use filter that only emits light from one of the dyes at a time.

Experimental: Fluorescence microscopy was used for ALP staining. The scaffolds were first prepared for imaging as described in subsection 3.2.3, and subsequently imaged using the inverted fluorescence microscope, Olympus IX71. ELF 97 has an excitation of 345 nm and emission of 530 nm (as seen in Figure 3.4), and therefore require a longpass filter set. The supplier of ELF 97, Thermo Fisher, recommends using a typical DAPI/Hoechst longpass filter set. Since Draq5 emits lights in the far-red region (seen in figure 3.4) a red laser was used, combined with a 650 LP filter.

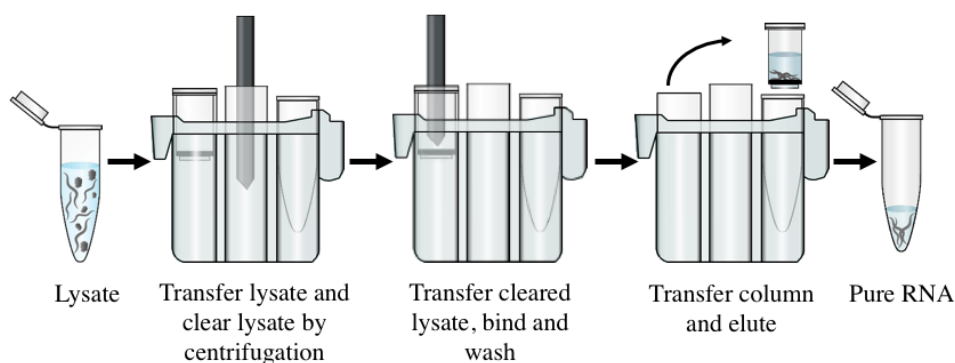


Figure 3.5: RNA isolation using QIAcube

The lysed sample is transferred to a spin column in a rotor adapter and cleared. Subsequently the cleared lysate is transferred again for binding, and finally washed to remove contaminants. The final step is the elution of the isolated RNA.

Immediately before imaging, a small amount (70 μL) of the ELF 97 solution was evenly distributed on the scaffold. The reaction occurs very fast, and it rarely takes longer than 5 minutes. The fluorescent precipitate is very photostable, and can withstand long periods of visualization. The characterization was done with a 20X magnification.

3.2.5 PCR Analysis

Principle: Polymerase Chain Reaction (PCR) is one of the most common techniques used in molecular biology. It is a quick way to amplify quantities of DNA to obtain millions of copies of DNA molecules. One cycle consists of three steps. The first step of the analysis is denaturation, where the sample is heated to a high temperature to separate the double stranded DNA into single strands. The next step is annealing, where the primers anneal to the denatured template DNA. The final step is extension (or replication) of new DNA strands by DNA polymerase. This cycle is repeated 40 times.

3.2.5.1 RNA Isolation

Principle: Before a reverse transcription real-time PCR analysis can be performed, pure RNA must be isolated. When a cell needs to produce a certain protein, the RNA activates the protein's gene and produces copies of that.

RNA isolation can be done both manually and automated. By using QIAcube, it is possible to run the isolation automated. Figure 3.5 explains the steps in the

RNA isolation using QIAcube together with RNeasy Mini QIAcube Kit. This automated method provides a fast, easy and convenient RNA purification, by centrifuging, washing, binding and eluting [78].

Experimental: Cells were harvested at set points (0 d, 7 d, 14 d and 21 d). Prior to lysing the cells, the medium was first completely removed. To avoid any contamination from the medium in the lysate, the scaffolds were also washed with PBS. The cells were lysed using a lysis buffer (350 μ L, Buffer RLT, QIAGEN). When the cells were lysed, it was important to make sure that all the cells inside the scaffolds were lysed, therefore a pipette was used to wash the scaffold several times with the buffer. The lysate was transferred to a 2 mL collection tube for RNA isolation. The RNA was isolated following the handbook of QIAcube using a RNA isolation kit (RNeasy Mini QIAcube Kit, QIAGEN). The settings used for the QIAcube was RNA protocol, RNeasy Mini, Animal tissue and cells, and DNase digest. The RNA was eluted in 30 μ L.

RNA concentration was measured using a spectrophotometer (NanoDrop 1000, Thermo Fisher Scientific). The RNA was stored at -80°C .

3.2.5.2 cDNA Synthesis and PCR Analysis

Principle: cDNA synthesis, also known as reverse transcription, produces complementary DNA (cDNA), by using RNA as a template. By reverse transcription, the RNA sequences can be converted to cDNA sequences. By combining reverse transcription with PCR, it is possible to detect RNA even at very low levels [79].

Experimental: cDNA was synthesized by reverse transcription using the High-Capacity RNA-to-cDNATMKit (ThermoFisher). A mix of RT Buffer Mix (10 μ L), RT Enzyme Mix (1 μ L) and RNA target (up to 9 μ L). Nuclease-free H₂O was added to get a total volume of 20 μ L per sample. This was briefly centrifuged and then incubated (37°C , 60 min). The reaction was stopped by heating (95°C , 5 min), and then the temperature decreased (4°C , ∞). The samples were stored in a freezer (-20°C) until used.

PCR analysis was done using a real-time PCR system (StepOnePlusTMReal-Time PCR System, Thermo Fisher). cDNA was diluted using nuclease-free H₂O, in order to have the same amount of cDNA for each target. Diluted cDNA (4 μ L) was added to a 96-well reaction plate (MicroAmp[®] Fast Optical 96-Well Reaction Plate, Applied Biosystems[®], Thermo Fisher). In addition, Master Mix (10 μ L, TaqMan[®] Universal PCR Master Mix, Applied Biosystems[®], Thermo Fisher), nuclease-free

H₂O (5 μ L), and probe (1 μ L). The probes used for detection of osteogenic phenotype were Osterix (Hs00541721_m1 *SP7*), RUNX-2 (Hs00231692_m1 *RUNX2*), Osteocalcin (Hs01587814_g1 *BGLAP*), Collagen type I (Hs00164004_m1 *COL1A1*) and Sclerostin (Hs00228830_m1 *SOST*). Gene expression were analyzed using the $\Delta\Delta$ CT method with the housekeeping gene glyceraldehydes-3-phosphate dehydrogenase (Hs99999905_m1 *GAPDH*), as an endogenous control.

3.2.6 Alizarin Red Staining

Principle: Alizarin red (ARS) staining is used in order to evaluate the calcium deposition. It was previously established in subsection 1.2.1, Bone Structure, that osteoblasts that are buried in the bone matrix, make and deposit, a protein mixture called osteoid. Eventually the mature osteoblasts deposit minerals, including calcium, into the osteoid to make bone. This calcium deposition can be evaluated by using ARS staining.

Experimental: The scaffolds and controls were seeded with BMSCs. At day 21 the cells were fixed as described in subsection 3.2.1.4, Fixation. Prior to ARS staining, the scaffolds were washed with both PBS and H₂O. Then, the scaffolds were incubated with ARS (40 mmol, 1 h, RT). After staining, the scaffolds were washed 10 times with H₂O. Pictures were taken with in an inverted light microscope using a mounted SLR camera. The scaffolds were destained using cetylpyridinium chloride (CPC, 10% (wt/vol)) in sodium phosphate buffer (10 mmol, pH=7, 1 h, RT). The supernatant was transferred to a 96-well plate and scanned in the Microplate Absorbance Reader in triplicates (570 nm, 30 μ L, iMark®, Bio-Rad Laboratories).

4 | Results

This chapter will present the results from the experimental work, as described in chapter 3, Experimental Methods. The highlights of the results will be mentioned, and then further discussed in chapter 5, Discussion.

4.1 Manufactured Scaffolds

As mentioned in section 3.1.1, Scaffold Design and Manufacturing, the scaffolds were manufactured using EBM, by the AM group FIT AG. Figure 4.1 shows the manufactured scaffolds, where (a) and (b) are the large opti and large scaffolds, and figure (c) is the small scaffold.

The porosities of the manufactured scaffolds were calculated using equation 3.2. The density was found to be $\sim 4.42 \text{ g/cm}^3$, this was found by measuring the density of the AM solid Ti control. The density is fairly similar to the density of annealed Ti-6Al-4V, which have a density of 4.43 g/cm^3 [80]. By using the density and the measured weight, height and diameter of the scaffolds, the porosity was found. Table 4.1 show the volumes and porosities for the scaffolds. The data given below "*Design*" are the data retrieved from the CAD, while the data given below "*Measured*" are the calculated data from the manufactured scaffolds. The "large" is the large scaffold, the "large opti" is the large opti scaffold, and the small is the small scaffold.

As seen in the table, the porosities for the manufactured scaffolds are higher than for the porosities found by using the CADs. The manufactured scaffolds have higher porosities due to building defects and powder particles containing entrapped gas [55].

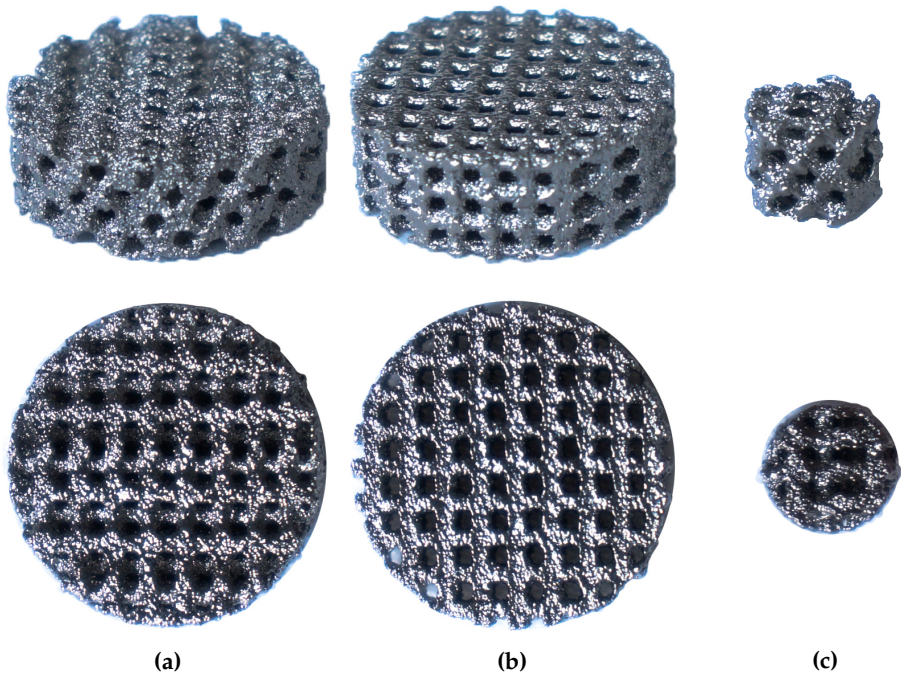


Figure 4.1: The manufactured scaffolds used for cell culturing
Scaffold (a) and (b) are the 24-well scaffolds, and scaffold (c) is the 96 well scaffold. The images were taken with a camera mounted on a tripod.

Table 4.1: Calculated and measured volumes and porosities of the scaffolds
The table show the calculated and measured porosities of the scaffolds. The data below *Design*, are the calculated data from the CADs, and the data below *Measured* are the measured data from the manufactured scaffolds.

	Large	Large opti	Small
Design			
Solid Volume (mm ³)	389	383	61
Total Volume (mm ³)	837	837	141
Porosity (%)	53	54	57
Measured			
Solid Volume (mm ³)	364	331	58
Total Volume (mm ³)	866	878	135
Porosity (%)	58	62	57

4.2 Metabolic Activity

To see if the cells were able to adhere and proliferate when cultured on the Ti controls, the alamarBlue® assay was used. By using this assay, it is possible to measure the metabolic activity of the BMSCs. The metabolic activity for the Ti controls had to be found, in order to use the results from the Ti controls as comparable results to the scaffolds.

Figure 4.2 shows the metabolic activity of the BMSCs cultured on Ti controls. Both controls express a steady increase in cell activity, where the BMSCs cultured in OM show a significantly higher metabolic activity. This indicate that the cells cultured with OM are differentiating as well as proliferating.

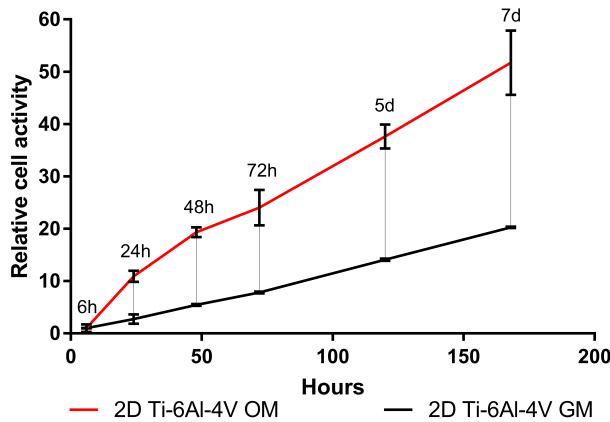


Figure 4.2: AlamarBlue® results of Ti controls

The graph is showing the alamarBlue® assay results. The results were normalized with respect to the first results at 6h.

4.3 Alkaline Phosphatase Activity

To determine differentiation of BMSCs to osteoblasts, cells, cultured on small scaffolds, were stained with ALP at day 10. Cells differentiating should show ALP activity already at day 7-10.

As expected, cells cultured in OM show higher ALP activity compared with cells cultured in GM, as shown in figure 4.3.

The images far to the left show the cell nuclei stained from Draq5™(red), the images in the middle are from ELF97®, that show the ALP activity of osteoblast cells. The images to the right are the merged images, with both Draq5™and ELF97®. The strongest red and green colors are where the images are in focus. Here the red and the green stains intersect. The co-localizations are shown as yellow.

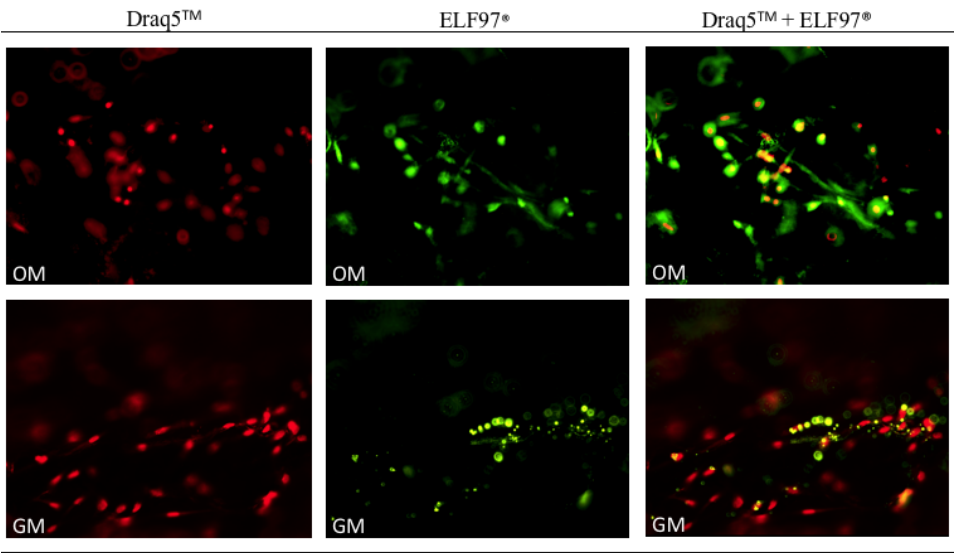


Figure 4.3: Fluorescence micrographs after ALP and Draq5 staining

The figure shows the results after ALP and Draq5 staining. The top row is the scaffold cultured with OM, and the bottom row is cultured with GM. Draq5™(red) was used to stain nuclei, and ELF97 was used to stain the ALP activity. The micrographs at the right show the merged micrographs. The yellow color indicates co-localization. The objective is set to a magnification of 20X.

4.4 PCR Analysis

Two experiments of PCR analysis was performed. Both experiments were done with 4 set time points (0d, 7d, 14d and 21d).

4.4.1 Experiment 1

The first experiment was performed with the large opti scaffolds for microscopy (30° angle), and blank controls.

4.4.1.1 RNA Concentration

The RNA concentration is shown in table 4.2. The RNA concentrations of the cells cultured on the scaffolds are very low compared to the 2D RNA concentration. Because of the low concentration, 2 ng cDNA had to be used for the PCR analysis. The cells lysed at day 21, cultured with GM on the large opti scaffold, have a 260:280 ratio below 2.00 (1.73), this may indicate impurities in the RNA.

Table 4.2: RNA concentration

The table shows the RNA concentration measured with NanoDrop after RNA isolation. The 2D samples are the blank controls, and the 3D samples are the large opti scaffolds.

Sample ID	RNA-conc [ng/ μ L]	260:280 ratio
Day 0	413.2	2.00
2D, Day 7, OM	183.42	2.09
2D, Day 7, GM	65.46	2.18
2D, Day 14, OM	109.02	2.04
2D, Day 14, GM	127.32	2.05
2D, Day 21, OM	150.9	2.07
2D, Day 21, GM	100.69	2.07
3D, Day 7, OM	20.78	2.08
3D, Day 7, GM	11.82	2.13
3D, Day 14, OM	20.28	2.15
3D, Day 14, GM	14.51	2.05
3D, Day 21, OM	34.42	2.09
3D, Day 21, GM	6.89	1.73

4.4.1.2 Collagen Type I

Collagen Type I is an osteoblast marker. Due to this it is expected an increase in this gene over the 21 days for the cells cultured with OM.

Figure 4.4 shows the expressions of COL1A1. The Y values are the relative quantification (RQ) values. These results are the changes in the gene expression of collagen type I relative to the reference gene (GAPDH). The X values are the set time points, measured in days. The results have been normalized with respect to sample 2D, Day7, OM.

The plot clearly shows a decrease in the gene of both scaffolds, from day 0 to day 7. After day 7, there is an evident increase in the gene for the cells cultured in the large opti scaffold, with GM (3D GM, black solid line). This expression is considerably higher compared to the cells cultured on the scaffold with OM (3D OM, red solid line).

The blank control cultured with OM (2D OM, red dotted line) express a steady increase of collagen type I, until day 14 to 21, where expression decreases.

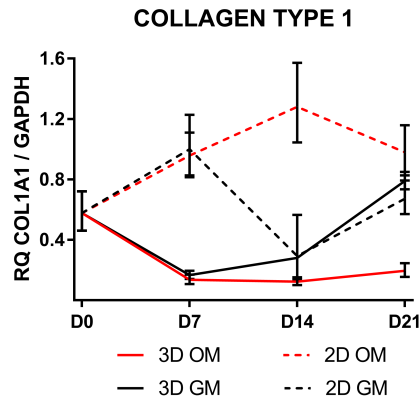


Figure 4.4: Gene expressions for Collagen type I

The plot shows the gene expressions for Collagen Type I, where the dashed lines are for the blank controls, and the solid lines are for the large opti controls. The results have been normalized with respect to 2D, Day7, OM.

4.4.1.3 RUNX2

The transcription factor, *RUNX2*, is a master switch for osteoblast differentiation. It is expected that the levels of *RUNX2* gradually increases in subsequent stages of osteoblast differentiation with maximum expression in mature osteoblasts.

Figure 4.5 show the expressions of *RUNX2*. These results are quite similar to the results for collagen type I, with maximum signal at day 14 for blank control, OM (2D OM, red dotted line), and a higher gene expression for the 24-well optimized scaffold cultured with GM. The biggest difference between *RUNX2* and *COL1A1*, is the decrease from day 0 to day 7 for 2D OM and 2D GM.

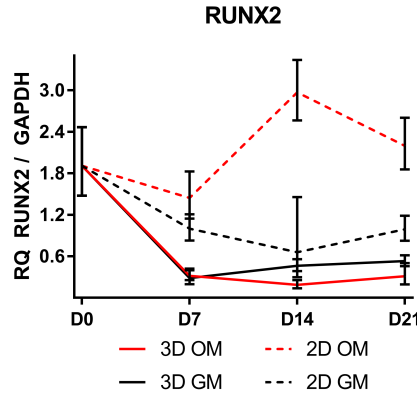


Figure 4.5: Gene expressions for RUNX2

The plot shows the gene expressions for *RUNX2*, where the dashed lines are for the blank controls, and the solid lines are for the large opti controls. The results have been normalized with respect to sample 2D, Day 7, OM.

4.4.1.4 Osterix

Osterix (SP7) is a DNA-binding transcription factor, and it is absolutely required for osteoblast differentiation. The gene expression of osterix is expected to increase during osteoblast maturation [81].

Figure 4.6 shows the expressions of osterix. Sample 2D OM express a high and increasing signal of osterix. Sample 2D GM also expresses an increasing signal, this is not nearly as high as the 2D sample cultured with OM. The expressions of the scaffolds are very low at day 21. The signal could not be detected at day 7 and day 14.

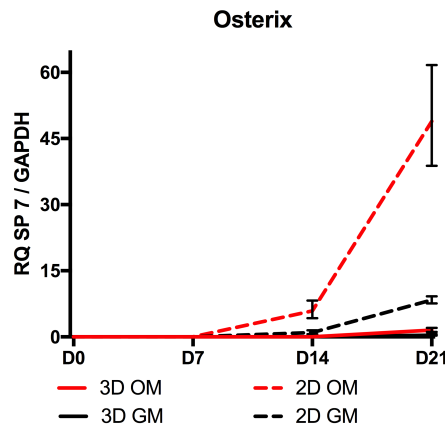


Figure 4.6: Gene expression for Osterix

The plot shows the gene expression for Osterix, where the dashed lines are for the blank controls, and the solid lines are for the large opti controls. The results have been normalized with respect to 2D, Day7, OM.

4.4.1.5 Osteocalcin

Osteocalcin is a non-collagenous protein component of bone that is produced by osteoblasts. Osteocalcin is expressed mainly in mature osteoblasts and pre-osteocytes. Figure 4.7 show the expression of osteocalcin. The results have been normalized with respect to sample 2D, Day7, OM.

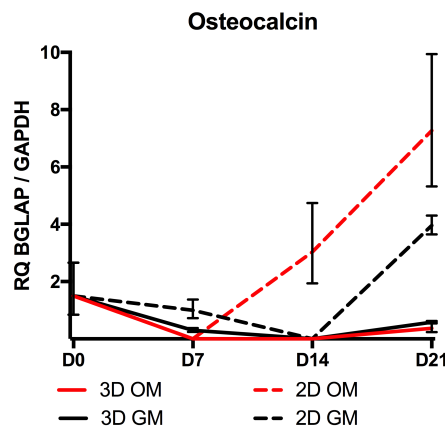


Figure 4.7: Gene expression for Osteocalcin

The plot shows the gene expression for Osteocalcin, where the dashed lines are for the blank controls, and the solid lines are for the large opti controls. The results have been normalized with respect to 2D, Day7, OM.

4.4.2 Experiment 2

The second experiment was performed with large scaffolds (0° optimization), Ti controls and blank controls. The two latter were cultured in 6-well plates. The non-optimized scaffolds were used in order to see if it could be the lysing of the cells that was the problem for the previous experiment.

4.4.2.1 RNA Concentration

The RNA concentration is shown in table 4.3. The samples named 2D, are the blank controls, the samples named 2DTi, are the Ti controls, and the 3D samples are large scaffolds. Note that this is not the same type of scaffold as the first experiment, where the scaffolds used there were the large opti scaffolds. See figure 3.3 for explanation of the referring names of the scaffolds/controls.

Table 4.3: RNA concentration

The table shows the RNA concentration measured with NanoDrop after RNA isolation. The 2D samples are the blank controls, 2DTi samples are the Ti control and the 3D samples are the large scaffolds. The RNA concentrations for the cells cultured on the scaffolds are very low compared to the RNA concentrations of the cells cultured on the controls. Because of the low concentrations, 1 ng cDNA had to be used for the PCR analysis.

Sample ID	RNA-conc [ng/ μ L]	260:280 ratio
Day 0	559.3	2.12
2D, Day 7, OM	39.1	2.08
2D, Day 7, GM	87.8	2.08
2D, Day 14, OM	85.6	2.11
2D, Day 14, GM	131.3	2.06
2D, Day 21, OM	313.6	2.05
2D, Day 21, GM	176.1	2.08
3D, Day 7, OM	47.8	2.02
3D, Day 7, GM	40.3	2.16
3D, Day 14, OM	6.5	2.47
3D, Day 14, GM	4.2	2.57
3D, Day 21, OM	7.6	2.17
3D, Day 21, GM	7.0	1.83
2DTi, Day 7, OM	15.6	2.04
2DTi, Day 7, GM	33.2	2.08
2DTi, Day 14, OM	74.8	2.09
2DTi, Day 14, GM	48.2	2.07
2DTi, Day 21, OM	24.8	2.21
2DTi, Day 21, GM	97.8	2.06

The cells lysed at day 21, cultured with GM on the large scaffold, have a 260:280-ratio below 2. This is the same sample as the previous experiment, which also had a ratio below 2. There are also several samples that have an abnormal

high 260:280 ratio. Pure RNA should have a ratio of ~ 2.0 , so a ratio of 2.57 is very high.

The RNA concentration is very low for many of the cells cultured on the 24-well scaffold samples. The lowest value is for the cells lysed at day 14, and cultured with GM on 24-well scaffold. This sample also had the highest 260:280 ratio, so it might be a correlation between the abnormally high 260:280 ratio, and the low RNA concentration.

Since the RNA concentrations are so low, it was necessary to use 1 ng cDNA for the PCR analysis. Due to the low amount of cDNA, it might be difficult to get a signal from the different genes.

4.4.2.2 Collagen Type 1

Figure 4.8 shows the expressions of COL1A1, where figure (a), is the large scaffolds, (b), is the blank controls, and (c), is the Ti controls. The Y values are the RQ values, *i.e.* the changes in the gene expression of collagen type I relative to the reference gene (GAPDH). The X values are the set time points, measured in days.

The results have been normalized with respect to day 0. The expression for the 24-well scaffold, cultured with GM had a maximum RQ value at day 14, and the scaffold cultured with OM has a steady growth after day 7. Both the 2D controls and the 2D Ti-6Al-4V controls have a maximum expression at day 7.

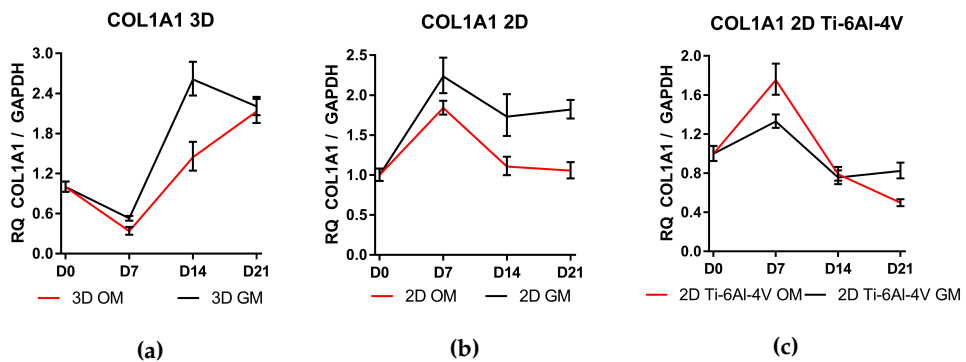


Figure 4.8: Gene expressions for Collagen type I

The plots show the gene expressions for Collagen Type I, where (a) is for the large scaffolds, (b) for the blank controls, and (c) is the gene expressions for Ti controls. The results have been normalized with respect to day 0.

4.4.2.3 RUNX2

Figure 4.9 shows the gene expressions for RUNX2. For every sample at each set time point, the expression is lower than for day 0. The expressions of the cells cultured on the scaffold/controls with GM are also generally higher than for the scaffold/controls cultured with OM. All though the expressions are generally very low for the cells, they still show a signal.

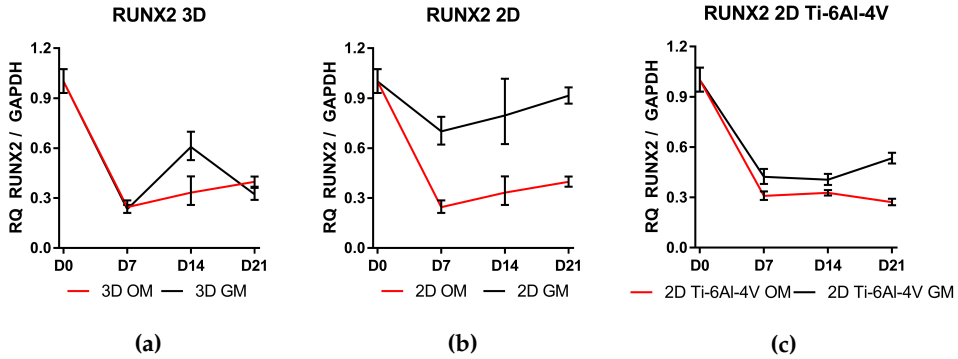


Figure 4.9: Gene expressions for RUNX2

The plots show the gene expressions for RUNX2, where (a) is for the large scaffolds, (b) for the blank controls, and (c) is the gene expressions for Ti controls. The results have been normalized with respect to sample day 0.

4.4.2.4 Osterix

Figure 4.10 show the gene expressions of osterix. For both the scaffolds and the 2D Ti-6Al-4V controls, the results are non-detectable at day 14. The cells cultured in the blank control, with GM, give the highest expression.

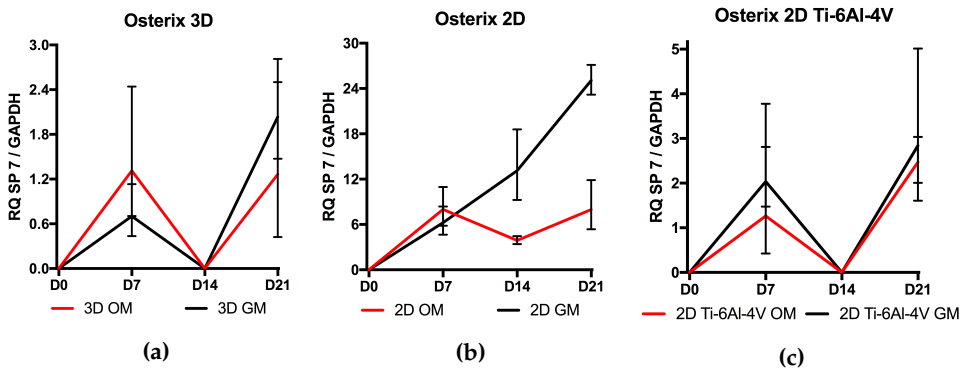


Figure 4.10: Gene expressions for Osterix

The plots show the gene expressions for Osterix, where (a) is for the large scaffolds, (b) for the blank controls, and (c) is the gene expressions for Ti controls. The results have been normalized with respect to Day 0.

4.4.3 Cycle Threshold Values

The cycle threshold (CT) values are the number of cycles required for the fluorescent signal to cross the threshold. Figure 4.11a show the mean, maximum and minimum CT values of the different gene expressions.

In figure 4.11b, the sclerostin expression is included. The relative quantification results from sclerostin are not included. This is due to the high CT value. CT values >35 were considered non detectable. The high CT values may infer contamination or background noise. Since the CT values were so high, the RQ values were neglected. The same applies for osteocalcin at Experiment 2. Since the CT values for osteocalcin were >35 , the RQ values were neglected. The amplification plots for the PCR analysis can be seen in Appendix 1.

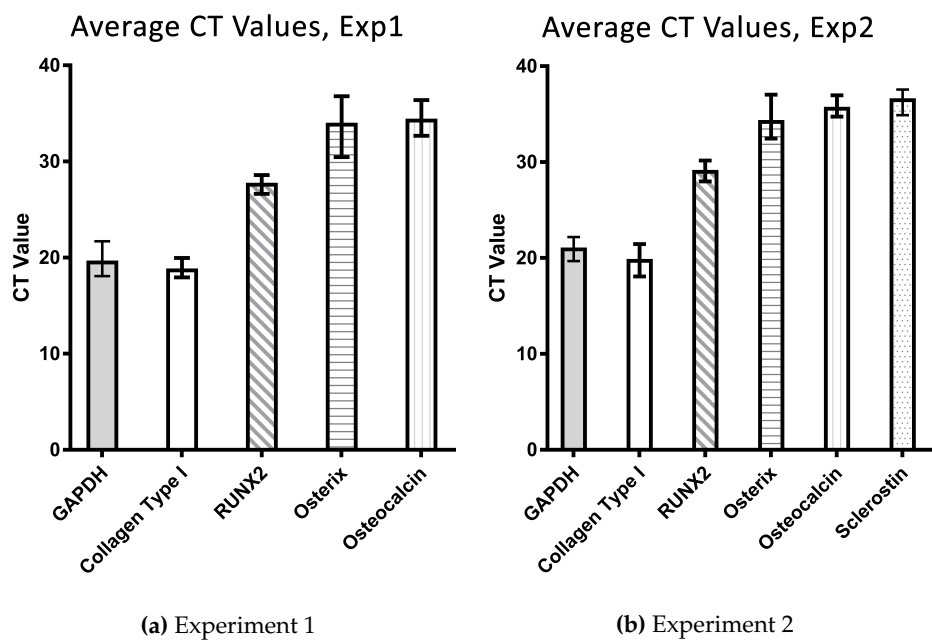


Figure 4.11: Mean, maximum and minimum CT values
Plot 4.11a shows the CT values from Experiment 1, including collagen type I, RUNX2, Osterix and Osteocalcin. Plot 4.11b shows the CT values from Experiment 2, including collagen type I, RUNX2, Osterix, Osteocalcin and Sclerostin.

4.5 Alizarin Red Staining

ARS staining was used to determine the calcium deposition, as a measurement of mature and functional osteoblasts.

The small, large and large optimized scaffolds, in addition to the Ti controls and blank controls, were used to investigate the calcium deposition. The calcium deposition of the cells cultured on the small scaffolds was investigated in two rounds. These rounds are labeled Run1 (R1) and Run2 (R2).

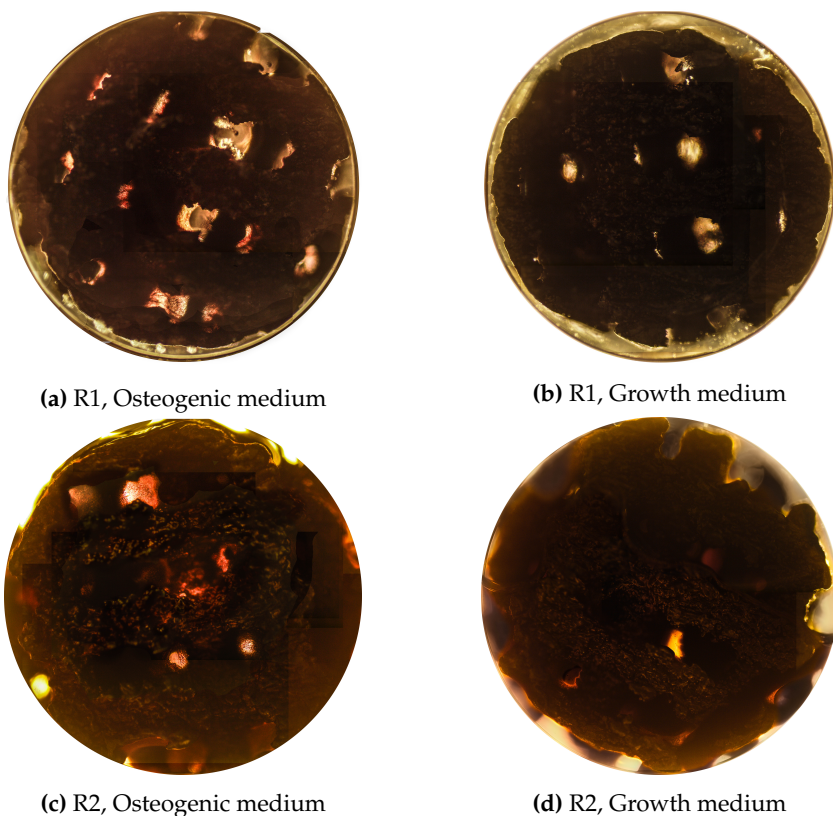


Figure 4.12: ARS staining of calcium deposition on small scaffold

Images from light microscopy, where scaffolds (a) and (c) are cultured with osteogenic medium, and (b) and (d) with growth medium. Images are taken with an inverted microscope (Olympus CKX41, Olympus Corporation) with a mounted SLR camera (Olympus E-620, Olympus Imaging Corporation), at 4X magnification.

The images were made up by taking several images using a mounted SLR camera on an inverted microscope at 4X magnification, and using a photo editing software (Photoshop CS6, Adobe) to combine the images into one picture. Since each

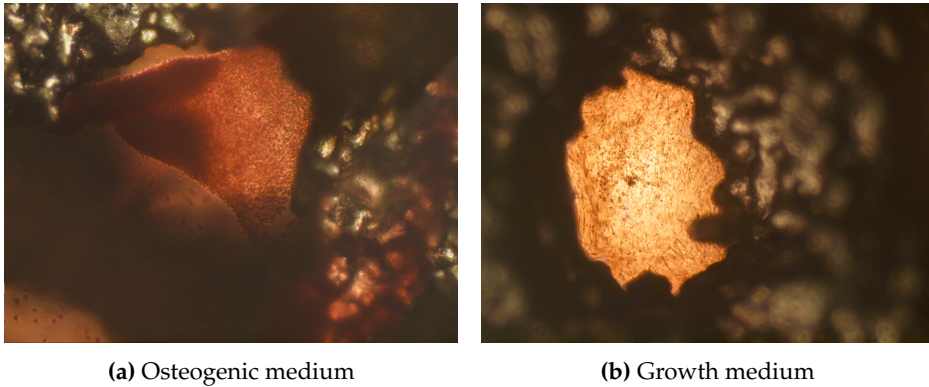


Figure 4.13: ARS staining of calcium deposition on large scaffolds

Images from light microscopy, where the large opti scaffold (a) is cultured with osteogenic medium, and (b), large scaffold, is cultured with growth medium. Images are taken with an inverted microscope (Olympus CKX41, Olympus Corporation) with a mounted SLR camera (Olympus E-620, Olympus Imaging Corporation), at 10X magnification.

picture taken with the SLR camera had different lighting, depending on where on the scaffold the image was taken, it was necessary with some brightness, contrast and exposure adjustments in order to get a good transition between the pictures.

Figure 4.13 shows images taken with the same camera and microscope as figure 4.12, at 10X magnification. The scaffold in figure 4.13a is a large opti scaffold cultured in OM, and the scaffold in figure 4.13b is a large scaffold cultured in GM. Both images are representative for the entire scaffold.

By looking closely in the right, bottom corner of figure 4.13a, it is possible to see a red staining on the surface of the scaffold. This indicate that the cells have adhered to the surface of the scaffold, as well as the pores of the scaffold. This red staining was visible on both the large scaffold and large opti scaffold.

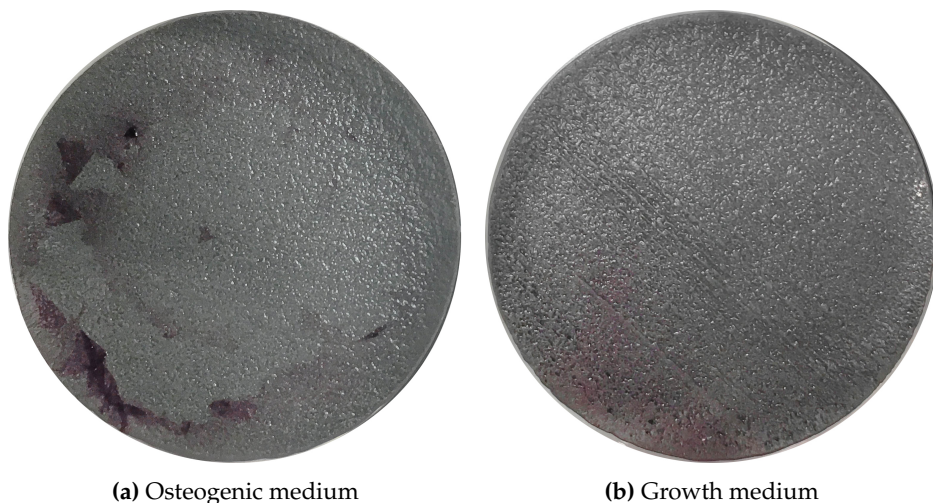


Figure 4.14: ARS staining of calcium deposition Ti control

The images show the ARS staining on Ti control, where control (a) is cultured with OM, and control (b) is cultured with GM. The images are taken with a hand-held camera.

Figure 4.14 show the ARS staining on the Ti controls. Since these controls are solid, it was not possible to take photos in an inverted microscope since there would not be enough light to see the staining. Therefore, the pictures of the controls were taken with a hand-held camera. The staining is shown in a dark red color, and it is easily seen in the control cultured with OM (figure 4.14a). By looking closely at the bottom part of the control cultured with GM (figure 4.14b), it is possible to see a red color from the staining.

All the images taken after staining show a much deeper and more noticeable red stain on the scaffolds/control cultured in OM. Although the staining in the scaffolds/control cultured with GM do not have a very prominent staining, there is still some tendency of staining.

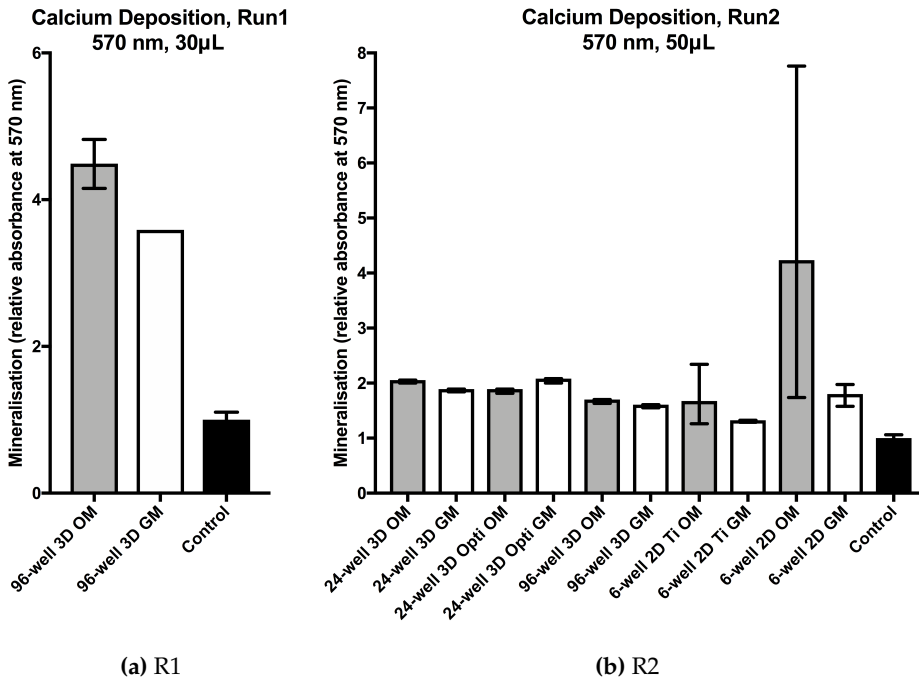


Figure 4.15: Calcium Deposition

The plots show the calcium deposition for (a), R1, and (b), R2. The mineralisation was detected at 570 nm in a 96-well, with 30 μ L for R1 and 50 μ L for R2. The absorbance values have been normalized with respect to a negative control.

Figure 4.15 show the calcium deposition for both (a), Run1, and (b), Run2. The absorbance values have been normalized with respect to a negative control (medium control). As seen in the graphs, the scaffolds/controls express a slightly higher calcium deposition when cultured with OM. This applies to all, except the large opti scaffold, where the scaffold cultured with GM has a slightly higher mineralization than the scaffold cultured with OM.

5 | Discussion

The biocompatibility of EBM manufactured Ti-6Al-4V scaffolds, with pore- and lattice- size 800 μm and porosity of $\sim 60\%$, have been investigated.

This chapter will discuss the results presented in the previous chapter, 4 Results. The two upcoming sections will discuss the biocompatibility and osteogenic properties of the scaffolds. The discussion will then move on to the effects of pore sizes and porosities. The final section will assess the challenges that occurred during this study.

5.1 Biocompatibility of Scaffolds

The biocompatibility of the scaffolds must be found in order to determine how compatible they are in a biological system. To discover if the scaffolds are fit for human use, the scaffolds were seeded with BMSCs *in vitro*. The scaffolds were compared to flat Ti surfaces. By doing so, it could be determined whether the scaffolds have a poorer biocompatibility compared to 2D structures with the same material. It is expected that the Ti-6Al-4V alloy serve a good biocompatibility, with cells adhering to the scaffolds, and subsequently start proliferating.

First, the metabolic activity of the BMSCs cultured on Ti controls was found by using the alamarBlue[®] assay. The results from the alamarBlue[®] assay are shown in figure 4.2. These results show a steady increase for both the control cultured with OM and the control cultured with GM. The control cultured with OM have a much higher relative cell activity than the control cultured with GM. This indicate that the cells have likely started to differentiate, in addition to proliferate. This is a reasonable assumption, since the osteogenic medium is designed to induce osteogenic differentiation.

The metabolic activity of the BMSCs cultured on scaffolds was previously discovered by Timothy Jørholm. The result, shown in figure 2.4, shows an increasing activity over time (9 d) for both the scaffold cultured in OM and the scaffold

fold cultured in GM. The scaffold cultured with OM also show a higher relative metabolic activity than the scaffold cultured with GM, similar to the results of the Ti controls. This too indicate the onset of differentiation, in addition to proliferation, of the BMSCs cultured with OM.

In order for cells to proliferate and differentiate, they must first find a surface to adhere to. Since the metabolic activity is increasing, then the cells must have adhered to the surfaces of the scaffolds/controls. However, this adhesion might not be so firm as it should be. By analyzing the staining results from ARS staining of the Ti controls (figure 4.14a), it is almost as if the cells have detached from the surface. There are reasons to believe that the Ti control surface was originally covered with cells. The figure show an evident stain near the edges of the control, while in the middle of the control, there is almost no stain at all. This may be due to cells detaching from the surface as a result of washing and fixation. It might also be because of a very high proliferation, leading to an overcrowd of cells. Resulting in the cells detaching of the surface, and grouping as large flakes of cells. Both assumptions suggest that the adhesion might not as firm as it should be. This could be further tested by using another donor, whose BMSCs do not proliferate as much.

It has now been established that the BMSCs do adhere and proliferate to the surface of the scaffolds. This result shows that EBM manufactured Ti-6Al-4V porous scaffolds offers a good biocompatibility. The next section will discuss the differentiation results of the cells cultured on the scaffolds.

5.2 Osteogenic Properties of Scaffolds

The osteogenic properties will tell how well the osseointegration of the implant will be. This can be characterized *in vitro* by finding the differentiation capacity of the cells when cultured on scaffolds.

The osteoblastogenesis can be detected by, among others, ALP staining. Alkaline phosphatase is an enzyme that is involved in the mineralisation of bone. When the ALP activity is high, it is an indication of osteoblast differentiation. Figure 4.3 shows the ALP staining of BMSCs cultured on small scaffolds. The fluorescent microscopy shows a signal for both the scaffold cultured with OM and the scaffold cultured with GM. The signal for the scaffold cultured with OM is, however, higher than for the scaffold with GM. The increased activity is associated with the differentiation of osteoblasts.

ELF-97 is a very sensitive technique. By allowing the reaction to continue too long, it can result in formation of large amounts of spurious background crystals.

Sometimes only seconds might be too long [82]. These can cause spontaneous crystal growth, and increase the non specific background signal [83, 84]. As seen in the middle of the micrograph for the scaffold cultured with GM (figure 4.3), the signal from the ELF97[®] is very strong compared to the rest of the micrograph. This might be due to crystal formation.

The ARS staining was used to evaluate the calcium deposits in the differentiated culture. Figure 4.12, 4.13 and 4.14 show the staining done after 21 days of incubation. Here it is easy to see that the scaffolds/control cultured with OM show a deeper red stain. Since mature osteoblasts deposit minerals, including calcium, the red stain indicate the presence of mature, functional osteoblasts. This is also inferred by the calcium deposition shown in the plots in figure 4.15. There was a higher mineralization for the scaffolds compared to the control. However, the mineralization for the BMSCs cultured in the blank controls, is much higher compared to the scaffolds. This indicate that the BMSCs cultured on the scaffolds do not differentiate as well as they do on the blank controls. It might also be because they were washed away due to poor adhesion, as explained in the previous section, 5.1, Biocompatibility of Scaffolds.

While the ALP and ARS staining indicate that the scaffolds induce osteoblastogenesis, the PCR analysis tell another story. The gene expressions found during the PCR analysis are, in general, lower for the scaffolds compared to the BMSCs cultured in the blank controls. In the second experiment of the PCR analysis, the results were compared to EBM manufactured 2D controls made by Ti-6Al-4V, the same material as the scaffolds. This comparison was reasonable to do in order to see if the results for the scaffolds were any different compared to the controls. The results for the Ti controls from both alamarBlue and the PCR analysis, are comparable to the results for the scaffolds. However, the RNA concentrations for the scaffolds are very low and decreasing over the three weeks, while the RNA concentrations for the Ti controls are higher and increasing at almost every time point, except day 21 OM, where the concentration decreased from 74.8 ng/ μ L (14 d), to 24.8 ng/ μ L (21 d).

The organic portion of bone consists largely of *collagen type I* [85]. Collagen type I also promotes the appearance of an osteoblastic phenotype by increasing in ALP activity and osteocalcin [86]. Collagen type I is expressed in all the samples, as shown in figure 4.4 and figure 4.8. The BMSCs cultured on the large opti scaffold with OM (First experiment, figure 4.4) have a gene expression lower than day 0 at every set time point. It is also not showing any significant increase. The other samples show an increase either at day 7 or day 14, and then the expression decreases. In general, the scaffolds/controls cultured with GM show a higher

expression than when cultured in OM. Since OM is used to induce the differentiation, then it is quite counterintuitive that the scaffolds/controls cultured in GM have a higher expression of collagen.

The transcription factor, *RUNX2*, is first detected in pre-osteoblasts, and then the expression increases as the cells start to differentiate. During the final stages of osteoblastogenesis, the expression should decrease [87]. This is because mature osteoblast do not express a significant amount of *RUNX2* protein. Figure 4.5 shows the expressions for *RUNX2* from the first experiment, and figure 4.9 shows the expression for *RUNX2* from the second experiment. Almost every sample shows an expression lower than the expression found at day 0. The cells cultured with OM generally show a lower expression, than for GM.

The results from the *COL1A1* and *RUNX2* genes for the scaffolds cultured in GM, do show a higher expression, compared to the scaffolds cultured in OM. Due to these result, the cells must have differentiated to osteoblasts. However, the *RUNX2* expressions for the scaffolds are significantly lower compared to Day 0. This means that the cells had more differentiated osteoprogenitor cells present before the cells were seeded to the scaffolds.

The DNA-binding transcription factor, Osterix, is expected to increase during osteoblast maturation. Here the expressions are very low for the cells cultured on the scaffolds and the Ti controls compared to the blank controls (Figures 4.6 and 4.10). The same applies for the non-collagenous protein, osteocalcin (Figure 4.7). It is expected an increase of osteocalcin with the presence of mature osteoblasts and pre-osteocytes. For both osterix and osteocalcin, the blank controls have a much higher expression than for the large scaffolds and Ti controls. This indicate that the osteoblasts for the scaffolds and the Ti have not differentiated to osteocytes.

No signal of the sclerostin gene was detected. Since sclerostin is produced by osteocytes, it can therefore be concluded that there are no osteocytes present in the scaffolds.

The results from *RUNX2* and collagen type I show that the cells have differentiated to osteoblasts. The same result is shown by the ALP staining. Osterix and osteocalcin have a lack of signal, this indicate that the osteoblasts have not reached its mature osteoblasts stage. The ARS staining, however, show the opposite. The staining show that the osteoblasts have indeed reached its mature osteoblast stage. Since the RNA concentrations are so low, and the 260:280 ratios are so abnormally high, then the results might have been affected of this. Therefore, the ARS staining is the most reliable result, and the problem for the abnormal RNA results might be when the cells were lysed. This is further discussed in section 5.4. To summarize, the cells cultured on the scaffolds have differentiated to mature osteoblasts. Due

to the lack of signal from sclerostin, it can be concluded that the osteoblasts have not differentiated to osteocytes.

5.3 Effects of Pore Size and Porosity

The scaffolds used in this research was designed with a pore size of 800 μm and a measured porosity of ~ 57 to 62 %. The previous sections in this chapter have explained that the scaffolds induce osteoblastogenesis, but not osteocytogenesis.

The research presented in section 2.3, State of the Art, shows that pore size greater than 150 μm up to 900 μm induce osteogenesis, *in vivo*. The experiments conducted in this thesis, *in vitro*, with pore size 800 μm , show that the scaffolds induce osteoblastogenesis, but the cells have not differentiated to osteocytes. However, if the cells were incubated longer, they might have differentiated to osteocytes. From the results from previous research, it can also be assumed that the cells would differentiate to osteocytes *in vivo*.

Scaffolds with high porosities have proven to induce osteogenesis. However, increasing porosities lead to a decrease in the mechanical properties of the scaffolds. The elastic modulus for the scaffolds used in this study was found to be 7.9 GPa for physical testing, and 16.9 GPa after a static compression using FEA. These results were obtained by Timothy Jøraholmen. Both results are within the region of human bone. A research done by C. Torres-Sanches et al. [88], show that porous Ti scaffolds with 55 % porosity, have an elastic modulus of 16.8 GPa. While a porous scaffold with 70 % porosity, have an elastic modulus of 6.2 GPa. These results agree with the results of the scaffolds used in this study.

The fatigue life of the scaffold still remains undiscovered. In addition, improved compression tests should be performed. This will be further discussed in chapter 7, Future Research.

5.4 Challenges

Many challenges occurred during the experimental work of this thesis. This section will highlight the most significant and important challenges that was faced during this work.

5.4.1 Cell Culturing

Before the cells were seeded to the intended surface, they were counted. The Bürker chamber is a simple approach, but it relies on experience, and it can therefore be quite inaccurate. If the cell suspension was not thoroughly mixed before added to the Bürker chamber, the total number of cells will be very inaccurate. Also, after the counting, the cells were centrifuged and then resuspended in the correct concentration. This usually leads to loss of cells, and therefore a lower concentration than first anticipated.

When the scaffolds were seeded with cells, it proved to be quite difficult to get the cells to go into the scaffold - instead of around it. This was most likely due to the viscosity of the medium. Even though the pores of the scaffolds are quite large, the medium created droplets on top of the scaffolds, instead of penetrating the scaffold. Because of this, it was inevitable that the cells adhered to the surface of the well. To avoid getting too many cells adhere to the well surfaces, the scaffolds, and Ti controls, were moved to new wells every seventh day.

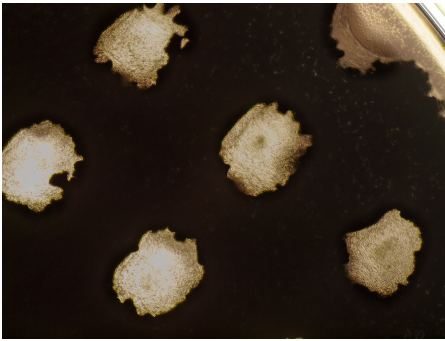
Moving the scaffolds

Moving the scaffolds, especially the small ones, was not easy. The scaffolds are designed to fit the 24- and 96-well plates, and it is therefore not much room to get a grip of the scaffolds with tweezers. In order to move the large scaffolds, the scaffolds were first tilted 90 degrees using a pipette, and then moved to new wells with sterile tweezers. The small scaffolds, however, had to be lifted up using two 0.5 mm × 16 mm hypodermic needles. The pores of the scaffolds were used as lifting points. Since the pores of the scaffolds are 0.8 mm, it was inevitable that some loss of cells would occur in the pores where the scaffolds were lifted.

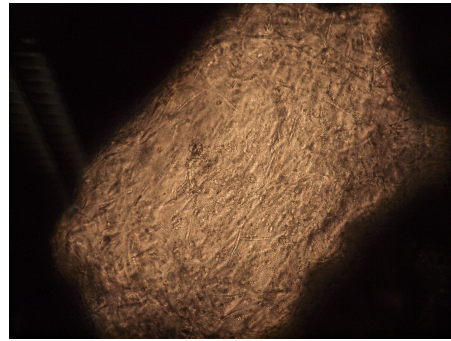
Sine the small scaffolds were used for microscopy (ARS staining and ALP staining), it was not ideal to use the pores to move the scaffolds. For the second run, it was decided to use a plate designed for adherent cells to not adhere to the well surface. This plate was used for the first 3 days, before the small scaffolds were moved to a 96-well plate. The new well plate was used for the rest of the incubation time.

Amount of cells

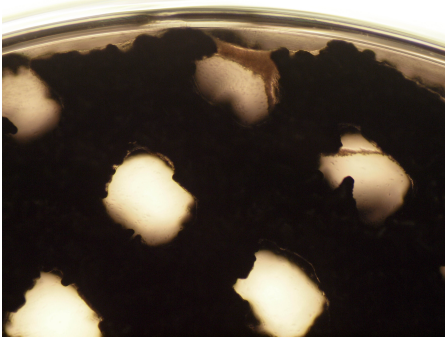
The amount of cells was quite variable. Some places there were so many cells that they grew as flakes, and eventually detached from the surfaces due to the amount of cells. Other places there were almost no cells present. This variation was quite large from scaffold to scaffold.



(a) ARS, GM, 4X Magnification



(b) ARS, GM, 10X Magnification



(c) PCR, GM, 4X Magnification



(d) PCR, GM, 10X Magnification

Figure 5.1: Variation of cell adhesion

The images show the cell adhesion on two different scaffolds. The scaffold type shown is the large scaffold. Both scaffolds are cultured with growth medium, and both scaffolds were supposedly seeded with the same amount of cells at the same time. The cells cultured on the scaffold shown in the images (a)-(b), were used for ARS staining. The cells cultured on the scaffold shown in the images (c)-(d), were used for PCR analysis.

Figure 5.1 shows a comparison of two scaffolds, both cultured with growth medium, and seeded with (supposedly) the same amount of cells at the same time. Here it is easy to see the big difference in cell growth. The cell growth on the scaffold shown in figure 5.1a-b has a significantly higher amount of visible cells. Here the visible cells are evenly distributed in the pores of the scaffold. The scaffold from figure 5.1c-d has almost no visible cells compared to the scaffold from figure 5.1a-b. There is, however, a chunk of cells in the top part of the scaffold. By comparing figure 5.1b with 5.1d, it is easy to see how much more evenly the cells are distributed in the scaffold used for ARS staining.

Cell Lysis

Prior to the PCR analysis, the cells were lysed using 350 μ L lysis buffer. This amount was a requirement for the RNA isolation. This was used to break down the membrane of a cell to compromise its integrity. However, 350 μ L is not enough to cover the scaffolds and controls, and therefore the scaffolds had to be "washed" several times using the same lysis. This made it difficult to make sure that all the cells had been properly lysed. It was especially difficult to make sure that the lysis had penetrated all the pores in the scaffold. In order to try to make the lysis process easier, the large scaffold was designed for the second experiment. Since there was no angle for the large scaffold, then it should be easier for the lysis to penetrate the pores. The result was at first promising with a higher RNA concentration, however, the RNA concentration decreased significantly during the subsequent readings. This might have been due to the cells detaching from the surface, and subsequently got removed when the medium was changed.

5.4.2 Microscopy Challenges

Microscopy, especially fluorescent microscopy, was not an easy task. The 3D structure of the scaffolds made it difficult to get a good focus inside the pores of the scaffold. Due to the 3D structure, it was inevitable to get a background signal with fluorescent microscopy. This is easy to see in figure 4.3.

The fluorescence signal of Draq5TM was first examined using a simplified automated imaging system (EVOSTMFL Auto 2 Imaging System, Invitrogen, Thermo Fisher Scientific). By using this imaging system, it was possible to do fully automated Z stacking of the scaffold, making it was possible to get a good focus of the signal throughout the pores of the scaffold, without any background signal.

Since the ELF97[®] assay required a longpass DAPI/Hoechst filter, it was not possible to use the simplified automated imaging system. Due to this, the focus had to be manually adjusted using an inverted fluorescence microscope (IX71, Olympus Europe GMBH, Hamburg, Germany), and it was not possible to get a Z-stack of the imaging.

It was not possible to use an inverted microscope to characterize the cell growth of the Ti controls during the cell culturing. This was because of the solid structure of the control, allowing no light to pass through. Because of this it was always unknown how many cells were present during the culturing. In order to validate

if the cells were present during the incubation time, and if the metabolic activity was high, they were tested by using the alamarBlue[®] assay. This gave a good result, with an increasing metabolic activity throughout the 7 days. However, it is still uncertain if any cells had detached from the surface, and subsequently got lost after changing the medium.

5.4.3 Cycle Threshold Values

The Cycle Threshold (CT) values are the number of cycles required for the fluorescent signal to cross the threshold. The quantitative PCR (qPCR) analysis in this experiment had 40 cycles. A low CT value indicate high amounts of target, while a high CT value indicate lower amounts of target. CT values below 29 show abundant target. If the sample has a qPCR CT value >35, it is considered not detectable, and the Relative Quantification (RQ) results are neglected (i.e. zero). CT values >35 may be a contamination. The gene expressions of Osterix (figure 4.6 and 4.10) and Osteocalcin (figure 4.7) both have a very high CT value. See figure 4.11a and 4.11b for the average, maximum and minimum values of the cycle threshold.

There are many factors that may influence the CT value. The factor that usually influences the most, is the concentration of the target. The CT value will increase with a decreasing amount of template [89]. This can be avoided by using more input total RNA, or to use a template at a lower dilution factor. The concentration used in this experiment was 2 ng cDNA for Run 1 and 1 ng cDNA for Run 2. This concentration is in the low range, and the reason for this was due to the low RNA concentration (ng/ μ L) given after the RNA isolation. Due to the low RNA concentration, it was not possible to get a template at a lower dilution factor. This had to be done to get enough samples for the PCR analysis.

However, the CT value for GAPDH is between 20-22, which is a reasonable value. The CT values are slightly higher for the second experiment. This can be explained because of the lower amount of cDNA (1 ng cDNA) compared to the first experiment (with 2 ng cDNA).

Another factor that influences the CT value is the master mix components. The fluorescence emission is proportional to the synthesized cDNA, and it can be affected by pH and salt concentration in a solution. This will result in a change in the reaction value.

Poor quality RNA is another factor that influences the CT value. This is probably the most important factor for this study. The quality of the RNA is examined when reading the RNA concentration with NanoDrop. A high quality RNA should have an A_{260}/A_{280} UV spectrophotometer reading close to 2. A ratio of

2.0 is considered pure RNA. If the ratio is lower it may indicate the presence of protein or other contaminants. At very low concentrations of RNA ($> 10 \text{ ng}/\mu\text{L}$) may also give inaccurate ratios, these ratios may either be higher or lower than 2.0. This can explain the high ratios from the second experiment, where the ratio is at most 2.57 (Large scaffold, Day 14, GM).

6 | Conclusion

Porous scaffolds, with pore- and lattice diameter of 800 μm and porosity of $\sim 60\%$, were designed and manufactured using EBM with material Ti-6Al-4V. The scaffolds were seeded with BMSCs. Immediately after being seeded with cells, the cells adhered to the surface of the scaffolds, and subsequently started proliferating. This infers that the EBM manufactured scaffolds are biocompatible.

The osteogenic properties of the scaffolds were also studied. The results obtained from the ALP staining, show an evident stain on the scaffolds. All though the BMSCs cultured with OM have a more distinct stain, there is still a clear signal of the BMSCs cultured with GM. Since ALP is an early marker of osteoblasts, then the high ALP activity infers the onset of osteoblastogenesis. In order to discover if the BMSCs had differentiated to mature osteoblasts, the ARS staining was used to stain the calcium deposition. The BMSCs cultured on the scaffolds with OM, show a deep red staining, and the BMSCs with GM also show a staining, this proves that mature osteoblasts are present in the culture.

The PCR analysis show a lack of signal of the osterix DNA-binding transcription factor and the non-collagenous osteocalcin protein. Due to abnormal RNA concentrations and A260/280 ratios, the PCR results for the scaffolds are considered inconclusive, and the results from ALP and ARS staining are the decisive factors in determining the osteoblastogenesis of the BMSCs cultured on the scaffolds. Since the sclerostin gene was undetectable during the PCR analysis, then it can be concluded that the osteoblasts did not differentiate to osteocytes.

In conclusion, the results suggest that Ti-6Al-4V porous scaffolds, with 800 μm pore size and $\sim 60\%$ porosity, induce the osteoblastogenesis of BMSCs *in vitro*, and are indeed biocompatible.

7 | Future Research

The list of future research is long. This is because I have recently signed a PhD contract with the intention to continue the research in this field. This section will therefore describe the future research plans within this topic.

An *in vitro* comparison of different pore sizes and porosities would be interesting to do. A research done by Jana Markhoff et al. [90] showed, *in vitro*, that scaffolds with smaller pores (400 μm to 620 μm) and a high porosity (75 %), expressed a higher metabolic cell activity and osteogenesis, compared to scaffolds with larger pore size 700 μm and lower porosity 51 %. Therefore it would be interesting to see if the scaffolds with smaller pores and higher porosity would enhance osteogenesis more by using the same BMSCs.

It would also be interesting to see if surface treatments (*i.e.* etching or bioactive coatings) will have a positive effect on the osteoconductive and osteoinductive properties. Lopez et al. [91] investigated the bone growth *in vivo* of etched porous scaffolds with porosity of around 60 %, and pore size diameter of 800 μm and 1200 μm . The scaffolds were etched in a mixture of acids consisting of nitric acid (HNO_3 50 %), fluorhydric acid (HF 40 %) and water (H_2O 10 %). The results showed an osseointegration through the implantation period.

In order to avoid cells adhering to the surface of the wells, ultra-low attachment well plates could be used (Corning®Costar®Ultra-Low Attachment Multiple Well Plate, Corning Inc). These plates are featured with a covalently bound hydrogel layer that inhibits cellular attachment. Because of this, the cells will only adhere to the surface of the scaffold. These plates are fairly expensive compared to the regular sterile plates, but by using these, the uncertainty of cells adhering to the well surfaces can be eliminated.

Cell adhesion can be enhanced by soaking the scaffolds with fibronectin prior to seeding the scaffolds with cells. A study done by Bruce E. Rapuano et al. [92] shows that cells cultured on Ti-6Al-4V disks, with preadsorbed fibronectin (1 nmol/L, 24 h), have an increased peak expression compared to untreated disks.

It would therefore be interesting to see if the differentiation would improve by preadsorbing the scaffolds with fibronectin.

The BMSC donor used for this thesis proved to have a very high proliferation capacity, resulting in an overcrowd of cells and formation of large flakes that eventually detached from the surface. It would therefore be beneficial to do a new experiment with another donor, preferably with a lower proliferation capacity, in order to give the cells room to differentiate. This might also enhance the adhesion of the cells.

An X-ray photoelectron spectroscopy (XPS) can be used in order to determine the element composition of the scaffolds, and if there are any elements that contaminate the surface after sterilization. The XPS results of an unsterile scaffold and a sterile scaffold should be compared, in order to see if there is any contamination present on the surface after sterilization. This will also determine if the alloy has the correct element composition.

Finally, if the research result in a biocompatible scaffolds with high osteogenic properties, the mechanical properties will be assessed. This will be assessed by mechanical testing, such as compression tests, to get the elastic modulus, and fatigue tests, to find its fatigue life. Some further modifications of the scaffolds might have to be made in order to get a favorable mechanical strength.

If the scaffold prove to induce osteogenesis, and exhibit a favorable mechanical strength, then the scaffold will be further researched, *in vivo*, in animals. First in rodents to prove the concept, and then larger animals to prove the concept in a load-bearing environment.

To summarize, these are the subjects that will be considered for future research:

- Comparison of different pore size and porosities, *in vitro*
- Surface treatments (*i.e.* etching or bioactive coating)
- Ultra-low attachment well plates to avoid cells adhering to well surfaces
- Cell adhesion with fibronectin preadsorbed scaffolds
- Conduct more experiments with a different donor, but same stem cell type
- X-ray photoelectron spectroscopy to determine the element composition and presence of contamination after sterilization
- Mechanical properties (Young's modulus, strength and fatigue life)
- *In vivo* research in small animal models.

Bibliography

- [1] Jae Young Rho, Richard B. Ashman, and Charles H. Turner. Young's modulus of trabecular and cortical bone material: Ultrasonic and microtensile measurements. *Journal of biomechanics*, 26:111–119, 02 1993. doi: 10.1016/0021-9290(93)90042-D.
- [2] KD Hunt, V Dean O'Loughlin, DW Fitting, and L Adler. Ultrasonic determination of the elastic modulus of human cortical bone. *Medical and biological engineering and computing*, 36(1):51–56, 1998. doi: 10.1007/BF02522857.
- [3] Subrata Pal. *Design of Artificial Human Joints & Organs*. Springer, 01 2014. ISBN 9781461462552.
- [4] Roger Narayan. *Biomedical Materials*. Volume 08. Springer, 2009. ISBN 978-0-387-84871-6.
- [5] Robert Mecham. *The extracellular matrix: an overview*. Springer Science & Business Media, 2011. ISBN 9783642165559.
- [6] Bruce Alberts. *Molecular biology of the cell*. Garland science, 2014. ISBN 0815345240.
- [7] Farshid Guilak, Leonidas G Alexopoulos, Maureen L Upton, Inchan Youn, Jae Bong Choi, Li Cao, Lori A Setton, and Mansoor A Haider. The pericellular matrix as a transducer of biomechanical and biochemical signals in articular cartilage. *Annals of the New York Academy of Sciences*, 1068(1):498–512, 2006. doi: 10.1196/annals.1346.011.
- [8] Josephine C Adams and Fiona M Watt. Regulation of development and differentiation by the extracellular matrix. *Development*, 117(4):1183–1198, 1993.
- [9] Per-Ingvar Brånemark. Introduction to osseointegration. *Tissue-Integrated Prosthesis: Osseointegration in Clinical Dentistry*, pages 11–76, 1985. doi: 10.1016/0022-3913(85)90460-3.

-
- [10] Celeste M Abraham. Brief historical perspective on dental implants, their surface coatings and treatments. *The open dentistry journal*, 8:50, 2014. doi: 10.2174/1874210601408010050.
- [11] Cuye Wien. *Surface Coating and Modification of Metallic Biomaterials*. 1st edition. Woodhead Publishing, 2015. ISBN 978-1-78242-303-4.
- [12] Roger Riley, David Williams, Micaela Ross, Shawn Zhao, Alden Chesney, Bradly D Clark, and Jonathan M Ben-Ezra. Bone marrow aspirate and biopsy: A pathologist's perspective. ii. interpretation of the bone marrow aspirate and biopsy. *Journal of clinical laboratory analysis*, 23:259–307, 01 2009. doi: 10.1002/jcla.20305.
- [13] Henk-Jan Prins. *Characterization of mesenchymal stem cells with in vivo bone forming capacity: "Bone building blocks"*. PhD thesis, University Utrecht, 2011.
- [14] John K. Fraser, Isabella Wulur, Zeni Alfonso, and Marc H. Hedrick. Fat tissue: an underappreciated source of stem cells for biotechnology. *Trends in Biotechnology*, 24(4):150 – 154, 2006. doi: 10.1016/j.tibtech.2006.01.010.
- [15] Tokiko Nagamura-Inoue and Haiping He. Umbilical cord-derived mesenchymal stem cells: Their advantages and potential clinical utility. *World journal of stem cells*, 6(2):195, 2014. doi: 10.4252/wjsc.v6.i2.195.
- [16] Joyce Doorn, Guido Moll, Katarina Le Blanc, Clemens van Blitterswijk, and Jan de Boer. Therapeutic applications of mesenchymal stromal cells: Paracrine effects and potential improvements. *Tissue Engineering Part B: Reviews*, 18(2):101–15, 04 2012. doi: 10.1089/ten.TEB.2011.0488.
- [17] Katarina Le Blanc et al. Mesenchymal stem cells for treatment of steroid-resistant, severe, acute graft-versus-host disease: a phase ii study. *Lancet*, 371:1579–86, 06 2008.
- [18] Robert D Steiner, Jessica Adsit, and Donald Basel. Col1a1/2-related osteogenesis imperfecta. *GeneReviews (Internet)*, 1, 1993-2018.
- [19] Edwin M Horwitz, Patricia L Gordon, Winston K K Koo, Jeffrey C Marx, Michael D Neel, Rene Y McNall, Linda Muul, and Ted Hofmann. Isolated allogeneic bone marrow-derived mesenchymal cells engraft and stimulate growth in children with osteogenesis imperfecta: Implications for cell therapy of bone. *Proceedings of the National Academy of Sciences of the United States of America*, 99(13):8932–7, 2002. doi: 10.1073/pnas.132252399.
-

-
- [20] Dario Siniscalco, James Jeffrey Bradstreet, Nataliia Sych, and Nicola Antonucci. Mesenchymal stem cells in treating autism: Novel insights. *World journal of stem cells*, 6(2):173–8, 2014. doi: 10.4252/wjsc.v6.i2.173.
- [21] Alok Sharma, Prerna Badhe, Nandini Gokulchandran, Pooja Kulkarni, Priti Mishra, Akshata Shetty, and Hemangi Sane. An Improved Case of Autism as Revealed by PET CT Scan in Patient Transplanted with Autologous Bone Marrow Derived Mononuclear Cells Stem Cell Research & Therapy. *Stem Cells International*, 3(2):2–5, 2013. doi: 10.4172/2157-7633.1000139.
- [22] Peter Connick et al. The mesenchymal stem cells in multiple sclerosis (MSCIMS) trial protocol and baseline cohort characteristics : an open-label pre-test : post-test study with blinded outcome assessments. *Trials*, 12(1):62, 2011. doi: 10.1186/1745-6215-12-62.
- [23] Carol Davila, Adriana Dulamea, and Fundeni Street. Mesenchymal stem cells in multiple sclerosis - translation to clinical trials. *Journal of Medicine and Life*, 8(1):24–27, 2015.
- [24] Corey J. Bishop, Jayoung Kim, and Jordan J. Green. Biomolecule Delivery to Engineer the Cellular Microenvironment for Regenerative Medicine. *Annals of biomedical engineering*, 42(7):1557–1572, 2014. doi: 10.1007/s10439-013-0932-1.Biomolecule.
- [25] Cameron J Wilson, Richard E Clegg, David I Leavesley, and Mark J Pearcy. Mediation of biomaterial–cell interactions by adsorbed proteins: a review. *Tissue engineering*, 11(1-2):1–18, 2005. doi: 10.1089/ten.2005.11.1.
- [26] Chris Niyibizi and David R. Eyre. Structural characteristics of cross-linking sites in type v collagen of bone. chain specificities and heterotypic links to type i collagen. *The FEBS Journal*, 224:943–50, 10 1994. doi: 10.1111/j.1432-1033.1994.00943.x.
- [27] J M Pace. A single amino acid substitution (d1441y) in the carboxyl-terminal propeptide of the proalpha1(i) chain of type i collagen results in a lethal variant of osteogenesis imperfecta with features of dense bone diseases. *Journal of Medical Genetics*, 39(1):23–29, Jan 2002. doi: 10.1136/jmg.39.1.23.
- [28] Patricia Ducy et al. Increased bone formation in osteocalcin-deficient mice. *Nature*, 382:448–52, 09 1996. doi: 10.1038/382448a0.
- [29] Kaisa K. Ivaska, Teuvo A. Hentunen, Jukka P Vääräniemi, Hannele Ylipahkala, Kim S I Pettersson, and H. Kalervo Väänänen. Release of intact
-

-
- and fragmented osteocalcin molecules from bone matrix during bone resorption in vitro. *The Journal of biological chemistry*, 279 18:18361–9, 2004. doi: 10.1074/jbc.M314324200.
- [30] Patricia Ducy, Rui Zhang, Valérie Geoffroy, Amy L Ridall, and Gérard Karsenty. Osf2/cbfa1: A transcriptional activator of osteoblast differentiation. *Cell*, 89(5):747 – 754, 1997. ISSN 0092-8674. doi: 10.1016/S0092-8674(00)80257-3.
- [31] Angela Oranger, Graziana Colaiani, and Maria Grano. *Bone Cells*, pages 3–13. Springer Milan, Milano, 2014. doi: 10.1007/978-88-470-5483-7_1.
- [32] Michaela Kneissel. The promise of sclerostin inhibition for the treatment of osteoporosis. *IBMS BoneKEy*, 6(7):259–264, 2009. doi: 10.1138/20090388.
- [33] Olivier Leupin, Elke Piters, Christine Halleux, Shouih Hu, Ina Kramer, Frederic Morvan, Tewis Bouwmeester, Markus Schirle, Manuel Bueno-Lozano, Feliciano J Ramos Fuentes, et al. Bone overgrowth-associated mutations in the *lrp4* gene impair sclerostin facilitator function. *Journal of Biological Chemistry*, 286(22):19489–19500, 2011. doi: 10.1074/jbc.M110.190330.
- [34] AH Burstein, DT Reilly, and M Martens. Aging of bone issue: mechanical properties. *The Journal of Bone & Joint Surgery*, 1976. doi: 10.2106/00004623-197658010-00015.
- [35] Hamdy Ibrahim, Sajedah Nasr Esfahani, Behrang Poorganji, David Dean, and Mohammad Elahinia. Resorbable bone fixation alloys, forming and post-fabrication treatments. *Materials Science and Engineering C*, 2016. doi: 10.1016/j.msec.2016.09.069.
- [36] Subcommittee: F42.91. Standard terminology for additive manufacturing technologies. Standard, ASTM International, Pennsylvania UnitedStates, March 2012.
- [37] Lore Thijs, Frederik Verhaeghe, Tom Craeghs, Jan Van Humbeeck, and Jean-Pierre Kruth. A study of the microstructural evolution during selective laser melting of ti–6al–4v. *Metals 2014*, 2010. doi: 10.1016/j.actamat.2010.02.004.
- [38] Arcam AB. *Arcam EBM Technology*. Arcam AB, n.a. URL <http://www.arcam.com/wp-content/uploads/arcamebm-corp-brochure-fnlv3.pdf>. Accessed 2018-03-20.
-

-
- [39] Swee Leong Sing, Jia An, Wai Yee Yeong, and Florencia Edith Wiria. Laser and electron-beam powder-bed additive manufacturing of metallic implants: A review on processes, materials and designs. *Journal of Orthopaedic Research*, 34(3):369–385, 2016. doi: 10.1002/jor.23075.
- [40] Manuela Galati and Luca Iuliano. A literature review of powder-based electron beam melting focusing on numerical simulations. *Additive Manufacturing*, 2017. doi: 10.1016/j.addma.2017.11.001.
- [41] Dirk Herzog, Vanessa Seyda, Eric Wycisk, and Claus Emmelmann. Additive manufacturing of metals. *Acta Materialia*, 2016. doi: 10.1016/j.actamat.2016.07.019.
- [42] Ian Gibson, David W. Rosen, and Brent Stucker. *Additive Manufacturing Technologies*. 1st edition. Springer, 2010. ISBN 978-1-4419-1119-3.
- [43] N Sykaras, a M Iacopino, V a Marker, R G Triplett, and R D Woody. Implant materials, designs, and surface topographies: their effect on osseointegration. A literature review. *The International journal of oral & maxillofacial implants*, 15(5):675–690, 2000.
- [44] Buddy D. Ratner, Allan S. Hoffman, Frederick J. Schoen, and Jack E. Lemons. A history of biomaterials. In *Biomaterials Science*, pages xli – liii. Academic Press, third edition edition, 2013. doi: 10.1016/B978-0-08-087780-8.00154-6.
- [45] J. J. Chalmers and M. Zborowski. *Magnetic Cell Separation*. Number v. 32 in *Laboratory Techniques in Biochemistry and Molecular Biology*. Elsevier Science, 2008. ISBN 9780444527547.
- [46] Carlos P Bergmann and Aisha Stumpf. Dental ceramics. *Biomaterials*, pages 9–11, 2013.
- [47] T.A. Dantas, C.S. Abreu, M.M. Costa, G. Miranda, F.S. Silva, N. Dourado, and J.R. Gomes. Bioactive materials driven primary stability on titanium biocomposites. *Materials Science and Engineering: C*, 77:1104 – 1110, 2017. doi: 10.1016/j.msec.2017.04.014.
- [48] Charles Godavitarne, Alastair Robertson, Jonathan Peters, and Benedict Rogers. Biodegradable materials. *Orthopaedics and Trauma*, 31(5):316–320, 2017. doi: 10.1016/j.mporth.2017.07.011.
- [49] Robert K. Schenk and Daniel Buser. Osseointegration: A reality. *Periodontology 2000*, 17(1):22–35, 1998. doi: 10.1111/j.1600-0757.1998.tb00120.x.
-

-
- [50] Lautenschlager EP and Monaghan P. Titanium and titanium alloys as dental materials. *International dental journal*, 43(3):245–53, 1993.
- [51] RR Boyer. An overview on the use of titanium in the aerospace industry. *Materials Science and Engineering: A*, 213(1-2):103–114, 1996. doi: 10.1016/0921-5093(96)10233-1.
- [52] Arcam AB. *Ti6Al4V Titanium Alloy*. Arcam AB, 2015. URL <http://www.arcam.com/wp-content/uploads/Arcam-Ti6Al4V-Titanium-Alloy.pdf>. Accessed 2018-03-20.
- [53] Arcam AB. *Arcam announces FDA clearance of implants produced with Additive Manufacturing*, 2012 (accessed May 2018). URL <http://www.arcam.com/arcam-announces-fda-clearance-of-implants-produced-with-additive-manufacturing/>.
- [54] Xiaoli Zhao, Shujun Li, Man Zhang, Yandong Liu, Timothy B. Sercombe, Shaogang Wang, Yulin Hao, Rui Yang, and Lawrence E. Murr. Comparison of the microstructures and mechanical properties of ti-6al-4v fabricated by selective laser melting and electron beam melting. *Materials and Design*, 2015. doi: 10.1016/j.matdes.2015.12.135.
- [55] Haize Galarraga, Diana A Lados, Ryan R Dehoff, Michael M Kirka, and Peeyush Nandwana. Effects of the microstructure and porosity on properties of ti-6al-4v alloy fabricated by electron beam melting (ebm). *Additive Manufacturing*, 10:47–57, 2016. doi: 10.1016/j.addma.2016.02.003.
- [56] Wei Quan Toh, Pan Wang, Xipeng Tan, Mui Ling Sharon Nai, Erjia Liu, and Shu Beng Tor. Microstructure and wear properties of electron beam melted ti-6al-4v parts: A comparison study against as-cast form. *Metals*, 6(11):284, 2016. doi: 10.3390/met6110284.
- [57] Joakim Karlsson, Mats Norell, Ulf Ackelid, Håkan Engqvist, and Jukka Lausmaa. Surface oxidation behavior of ti-6al-4v manufactured by electron beam melting (ebm®). *Journal of Manufacturing Processes*, 17:120–126, 2015. doi: 10.1016/j.jmapro.2014.08.005.
- [58] A Balamurugan, S Rajeswari, G Balossier, AHS Rebelo, and JMF Ferreira. Corrosion aspects of metallic implants—an overview. *Materials and Corrosion*, 59(11):855–869, 2008. doi: 10.1002/maco.200804173.

-
- [59] Oscar G Bodelón, Celia Clemente, Miguel Angel Alobera, Soledad Aguado-Henche, María Lorenza Escudero, and María Cristina García Alonso. Osseointegration of ti6al4v dental implants modified by thermal oxidation in osteoporotic rabbits. *International journal of implant dentistry*, 2(1):18, 2016. doi: 10.1186/s40729-016-0051-5.
- [60] Guifang Wang, Jinhua Li, Kaige Lv, Wenjie Zhang, Xun Ding, Guangzheng Yang, Xuanyong Liu, and Xinquan Jiang. Surface thermal oxidation on titanium implants to enhance osteogenic activity and in vivo osseointegration. *Scientific reports*, 6:31769, 2016. doi: 10.1038/srep31769.
- [61] B. Dutta and Francis H. Froes. The additive manufacturing (am) of titanium alloys. *Metal Powder Report*, 2017. doi: 10.1016/j.mprp.2016.12.062.
- [62] SF Hulbert, FA Young, RS Mathews, JJ Klawitter, CD Talbert, and FH Stelling. Potential of ceramic materials as permanently implantable skeletal prostheses. *Journal of Biomedical Materials Research Part A*, 4(3):433–456, 1970. doi: 10.1002/jbm.820040309.
- [63] Feng Bai, Zhen Wang, Jianxi Lu, Jian Liu, Gongyi Chen, Rong Lv, Jun Wang, Kaili Lin, Jinkang Zhang, and Xin Huang. The correlation between the internal structure and vascularization of controllable porous bioceramic materials in vivo: a quantitative study. *Tissue Engineering Part A*, 16(12):3791–3803, 2010. doi: 10.1089/ten.TEA.2010.0148.
- [64] Naoya Taniguchi, Shunsuke Fujibayashi, Mitsuru Takemoto, Kiyoyuki Sasaki, Bungo Otsuki, Takashi Nakamura, Tomiharu Matsushita, Tadashi Kokubo, and Shuichi Matsuda. Effect of pore size on bone ingrowth into porous titanium implants fabricated by additive manufacturing: an in vivo experiment. *Materials Science and Engineering: C*, 59:690–701, 2016. doi: 10.1016/j.msec.2015.10.069.
- [65] Johan Van der Stok, Olav P Van der Jagt, Saber Amin Yavari, Mirthe FP De Haas, Jan H Waarsing, Holger Jahr, Esther MM Van Lieshout, Peter Patka, Jan AN Verhaar, Amir A Zadpoor, et al. Selective laser melting-produced porous titanium scaffolds regenerate bone in critical size cortical bone defects. *Journal of Orthopaedic Research*, 31(5):792–799, 2013. doi: 10.1002/jor.22293.
- [66] Su-Hua Wu, Yi Li, Yong-Quan Zhang, Xiao-Kang Li, Chao-Fan Yuan, Yu-Lin Hao, Zhi-Yong Zhang, and Zheng Guo. Porous titanium-6 aluminum-4 vanadium cage has better osseointegration and less micromotion than a
-

-
- poly-ether-ether-ketone cage in sheep vertebral fusion. *Artificial organs*, 37 (12), 2013. doi: 10.1111/aor.12153.
- [67] Timothy Jøraholmen. Differentiation and bone deposition of bone marrow derived stem cells on additive manufactured porous ti-6al-4v scaffolds. Master's thesis, Norwegian University of Science and Technology, 06 2017.
- [68] Fit Production. *Medical Technology—Standard and Individual Implants*. FIT Production GmbH, n.a. URL <http://www.fit-production.de/medizintechnik.php>. Accessed 2018-05-20.
- [69] FIT Production GmbH. *Material data sheet for titanium parts produced by Electron Beam Melting*. FIT Production, 2015. URL http://www.fit-production.de/pdf/Materialdatenblatt/Materialdatenblatt_EBM_FIT_Production.pdf. Accessed 2018-03-20.
- [70] Mandana Mohyeddin Bonab, Kamran Alimoghaddam, Fatemeh Talebian, Syed Hamid Ghaffari, Ardeshir Ghavamzadeh, and Behrouz Nikbin. Aging of mesenchymal stem cell in vitro. *BMC cell biology*, 7(1):14, 2006. doi: 10.1186/1471-2121-7-14.
- [71] Victor Vacanti, Elton Kong, Gen Suzuki, Kazuki Sato, John M Canty, and Techung Lee. Phenotypic changes of adult porcine mesenchymal stem cells induced by prolonged passaging in culture. *Journal of cellular physiology*, 205 (2):194–201, 2005. doi: 10.1002/jcp.20376.
- [72] MONNIPHA Sila-Asna, Ahnond Bunyaratvej, Sakan Maeda, Hiromichi Kitaguchi, and NARONG Bunyaratavej. Osteoblast differentiation and bone formation gene expression in strontium-inducing bone marrow mesenchymal stem cell. *Kobe J Med Sci*, 53(1-2):25–35, 2007.
- [73] Seong-Oh Kim, Joonhui Kim, Takaharu Okajima, and Nam-Joon Cho. Mechanical properties of paraformaldehyde-treated individual cells investigated by atomic force microscopy and scanning ion conductance microscopy. *Nano Convergence*, 4(1):5, 2017. doi: 10.1186/s40580-017-0099-9.
- [74] D Hopwood. Cell and tissue fixation, 1972–1982. *Histochemical Journal - HISTOCHEM J*, 17:389–442, 04 1985. doi: DOI:10.1007/BF01003203.
- [75] Cecil H. Fox, Frank B. Johnson, John Whiting, and Peter P. Roller. Formaldehyde fixation. *The journal of Histochemistry and Cytochemistry*, 33:845–853, 04 1985. doi: 10.1177/33.8.3894502.
-

-
- [76] W. T. Mason. *Fluorescent and Luminescent Probes for Biological Activity : A Practical Guide to Technology for Quantitative Real-Time Analysis.*, volume 2nd ed of *Biological Techniques*. Academic Press, 1999. ISBN 9780124478367.
- [77] Mortimer Abramowitz and Michael W. Davidson. *Fluorescence Filters*. Olympus, 2018. URL <https://www.olympus-lifescience.com/en/microscope-resource/primer/techniques/fluorescence/filters/>. Accessed 2018-05-10.
- [78] Qiagen. *QIAcube® User Manual*. Qiagen, 2016. URL <https://www.qiagen.com/us/resources/download.aspx?id=f7d77c6e-0479-4b2b-a2e0-5ca747114e34&lang=en>. Accessed 2018-05-12.
- [79] Julia A Bridge. Reverse transcription–polymerase chain reaction molecular testing of cytology specimens: Pre-analytic and analytic factors. *Cancer cytopathology*, 125(1):11–19, 2017. doi: 10.1002/cncy.21762.
- [80] ASM aerospace specification metals. *Titanium Ti-6Al-4V (Grade 5), Annealed*. ASM aerospace specification metals, 2014. URL <http://asm.matweb.com/search/SpecificMaterial.asp?bassnum=MTP641>. Accessed 2018-03-20.
- [81] Yoshio Ohyama, Akira Nifuji, Yukiko Maeda, Teruo Amagasa, and Masaki Noda. Spatiotemporal association and bone morphogenetic protein regulation of sclerostin and osterix expression during embryonic osteogenesis. *Endocrinology*, 145(10):4685–4692, 2004. doi: 10.1210/en.2003-1492.
- [82] K D Larison, R BreMiller, K S Wells, I Clements, and R P Haugland. Use of a new fluorogenic phosphatase substrate in immunohistochemical applications. *Journal of Histochemistry & Cytochemistry*, 43(1):77–83, 1995. doi: 10.1177/43.1.7822768.
- [83] Gerhard W Hacker and Raymond R Tubbs. *Molecular morphology in human tissues: Techniques and applications*. CRC Press, 2004. ISBN 9780849317026.
- [84] Violette B. Paragas, Yu-Zhong Zhang, Richard P. Haugland, and Victoria L. Singer. The elf-97 alkaline phosphatase substrate provides a bright, photostable, fluorescent signal amplification method for fish. *Journal of Histochemistry & Cytochemistry*, 45(3):345–357, 1997. doi: 10.1177/002215549704500302.
- [85] Songtao Shi, Martin Kirk, and Arnold J Kahn. The role of type i collagen in the regulation of the osteoblast phenotype. *Journal of Bone and Mineral Research*, 11(8):1139–1145, 1996. doi: 10.1002/jbmr.5650110813.
-

-
- [86] L Masi, A Franchi, M Santucci, D Danielli, L Arganini, V Giannone, L Formigli, S Benvenuti, A Tanini, F Beghe, et al. Adhesion, growth, and matrix production by osteoblasts on collagen substrata. *Calcified tissue international*, 51(3):202–212, 1992. doi: 10.1007/BF00334548.
- [87] Toshihisa Komori. Regulation of osteoblast differentiation by runx2. In Yongwon Choi, editor, *Osteoimmunology*, pages 43–49, Boston, MA, 2010. Springer US. ISBN 978-1-4419-1050-9.
- [88] Carmen Torres-Sanchez, FRA Al Mushref, M Norrito, K Yendall, Yang Liu, and Paul P Conway. The effect of pore size and porosity on mechanical properties and biological response of porous titanium scaffolds. *Materials Science and Engineering: C*, 77:219–228, 2017. doi: 10.1016/j.msec.2017.03.249.
- [89] ThermoFisher Scientific. *Real-time PCR: understanding CT*, 2016. URL <https://www.thermofisher.com/content/dam/LifeTech/Documents/PDFs/PG1503-PJ9169-CO019879-Re-brand-Real-Time-PCR-Understanding-Ct-Value-Americas-FHR.pdf>. Accessed 2018-03-05.
- [90] Jana Markhoff, Jan Wieding, Volker Weissmann, Juliane Pasold, Anika Jonitz-Heincke, and Rainer Bader. Influence of different three-dimensional open porous titanium scaffold designs on human osteoblasts behavior in static and dynamic cell investigations. *Materials*, 8(8):5490–5507, 2015.
- [91] MA Lopez-Heredia, E Goyenvalle, E Aguado, P Pilet, C Leroux, M Dorget, P Weiss, and P Layrolle. Bone growth in rapid prototyped porous titanium implants. *Journal of biomedical materials research Part A*, 85(3):664–673, 2008. doi: 10.1002/jbm.a.31468.
- [92] Bruce E Rapuano, Kyle M Hackshaw, Hannes C Schniepp, and Daniel E MacDonald. Effects of coating a titanium alloy with fibronectin on the expression of osteoblast gene markers in the mc3t3 osteoprogenitor cell line. *The International journal of oral & maxillofacial implants*, 27(5):1081, 2012.

Acronyms

ALP	Alkaline Phosphatase.
AM	Additive Manufacturing.
ARS	Alizarin Red S.
ASD	Autism Spectrum Disorder.
BGLAP	Bone Gamma-Carboxyglutamate Protein, <i>Osteocalcin</i> .
BMSC	Bone marrow-derived Mesenchymal Stromal Cells.
CAD	Computer Aided Design.
COL1A1	Collagen Type I.
CP	Commercial Purity.
CPC	Cetylperidinium Chloride.
CT	Cycle Threshold.
DED	Directed Energy Deposition.
EBM	Electron Beam Melting.
ECM	Extracellular matrix.
FBS	Fetal Bovine Serum.
FEA	Finite Element Analysis.
GAPDH	Glyceraldehyde 3-Phosphate Dehydrogenase.
GM ₁	Growth Medium ₁ .
GM ₂	Growth Medium ₂ .
GvHD	Graft-versus-host disease.
HS	Human Serum.
LP	Longpass.
MS	Multiple Sclerosis.
MSC	Mesenchymal Stromal Cell.
OI	Osteogenesis Imperfecta.
OM	Osteogenic Medium.
PBF	Powder Bed Fusion.
PBS	Dulbecco's Phosphate Buffered Saline.
PCR	Polymerase Chain Reaction.
PFA	Paraformaldehyde.
PL	Platelet Lysate.

RNA	Ribonucleic acid.
RQ	Relative Quantification.
RUNX2	Runt domain-containing transcription factor.
SEM	Scanning Electron Microscopy.
SLM	Selective Laser Melting.
SLR	Single-lens Reflex.
SOST	Sclerostin.
SP	Shortpass.
SP7	Sp7 transcription factor, <i>Osterix</i> .

Glossary

adherent cell A specific cell type that adhere to surfaces, that require a specific subculturing. The growth of adherent cells are limited to the surface are. Media changes can be done by simply removing old media, and then added fresh media to.

biocompatibility The ability of a material to exist in harmony with tissue without causing deleterious changes.

bone graft A surgical procedure to repair extremely complex bone fractures.

differentiation he cell differentiation is the process where a cell changes from one cell type to another. Since the osteoprogenitor cell proliferate asymmetrically, then the cell with a predefined cell fate will differentiate to a final cell function, such as osteoblasts.

in vivo Performed or taking place in a living organism.

in vitro Performed or taking place outside a living organism.

multipotent Multipotency describes progenitor cells which have the gene activation potential to differentiate into discrete cell types.

osseointegration A direct contact between an implant and human bone.

osteoblast A cell type that arises from mesenchymal stem cells, and forms new bone.

osteoblastogenesis The production of osteoblasts.

osteoclast Bone cell that breaks down bone tissue.

osteocyte The differentiated product of osteoblasts.

osteogenesis The formation of bone.

osteoid Newly formed bone matrix before calcification.

osteon is a cylindrical structure that consists of concentric layers, lamellae, surrounding the central canal, known as haversian canal.

osteoprogenitor cell Cells that undergo metamorphosis to become an osteoblast.

proliferation Proliferation is a process that results in an increase of the number of cells. Once the adherent cells have adhered to the implant, the proliferation process initiates. Stem cells have the ability to proliferate both symmetrically and asymmetrically. When the stem cells proliferate symmetrically it is generated two new stem cells, whereas in asymmetrically proliferation it is generated both a new stem cell and a cell with a predefined cell fate. Osteoprogenitor cells proliferate asymmetrically.

trypsinize To dissociate adherent cells from the vessel in which they are being cultured.

List of Tables

1.1	Therapeutic applications of MSCs on different diseases	7
1.2	Element limits and mechanical properties for CP Ti	15
1.3	Mechanical properties of $\alpha - \beta$ Ti alloys	15
1.4	Comparison of EBM, SLM, wrought and cast fabricated Ti-6Al-4V .	16
3.1	EBM settings	31
3.2	Material data sheet for EBM manufactured Ti-6Al-4V	31
3.3	Referring of scaffolds and controls	32
4.1	Calculated and measured volumes and porosities of the scaffolds .	44
4.2	RNA concentration	47
4.3	RNA concentration	51

List of Figures

1.1	The bone structure of a long bone	3
1.2	Bone remodeling	4
1.3	Gene expressions during osteoblast-to-osteocyte ontogeny	8
2.1	The processes that affects the osteogenesis and mechanical properties	17
2.2	Close-up images of grains	21
2.3	Characterization of the surface by SEM	22
2.4	AlamarBlue® results	22
2.5	Fluorescent micrographs of the cell adhesion	23
2.6	Collagen Type I expressions	24
2.7	RUNX2 expressions	24
2.8	Osteocalcin expressions	25
2.9	Osterix expressions	25
2.10	Sclerostin expressions	25
2.11	Calcium deposition	26
3.1	Lattice structure	30
3.2	The designed scaffolds used for cell culturing	30
3.3	Grid pattern of a bürker chamber	35
3.4	Normalized excitation and emission spectra	38
3.5	RNA isolation using QIAcube	39
4.1	The manufactured scaffolds used for cell culturing	44
4.2	AlamarBlue® results of Ti controls	45
4.3	Fluorescence micrographs after ALP and Draq5 staining	46
4.4	Gene expression for Collagen type I	48
4.5	Gene expression for RUNX2	49
4.6	Gene expression for Osterix	50

4.7	Gene expression for Osteocalcin	50
4.8	Gene expressions for Collagen type I	52
4.9	Gene expressions for RUNX2	53
4.10	Gene expressions for Osterix	54
4.11	Mean, maximum and minimum CT values	55
4.12	ARS staining of calcium deposition on small scaffold	56
4.13	ARS staining of calcium deposition on large scaffolds	57
4.14	ARS staining of calcium deposition on Ti control	58
4.15	Calcium Deposition	59
5.1	Variation of cell adhesion	67

Appendix 1

Amplification Plots

Amplification Plots, Experiment 1

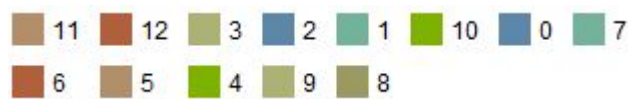


Figure 7.1: Color labeling

#	Name	#	Name
1	Blank, D7, OM	7	Large, D7, OM
2	Blank, D7, GM	8	Large, D7, GM
3	Blank, D14, OM	9	Large, D14, OM
4	Blank, D14, GM	10	Large, D14, GM
5	Blank, D21, OM	11	Large, D21, OM
6	Blank, D21, GM	12	Large, D21, GM

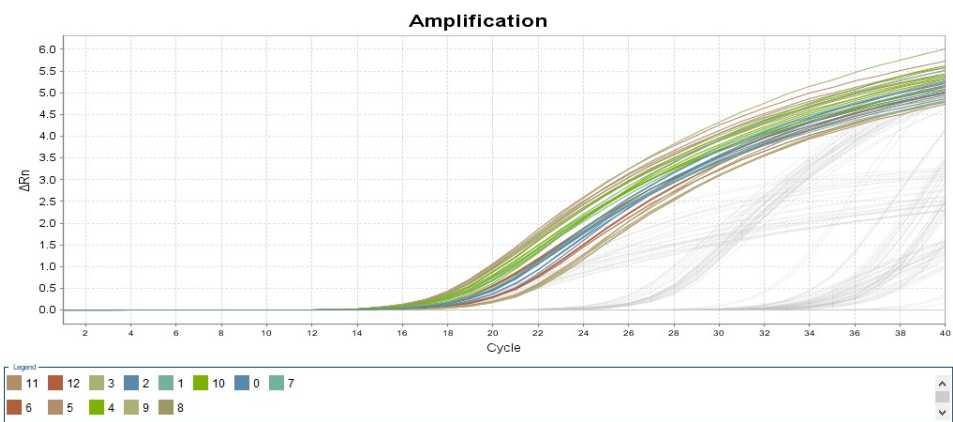


Figure 7.2: GAPDH Amplification plot, Experiment 1

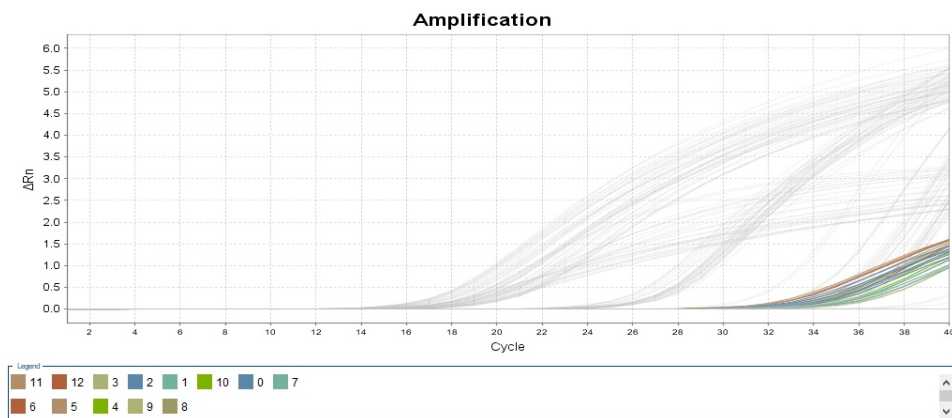


Figure 7.3: BGLAP Amplification plot, Experiment 1

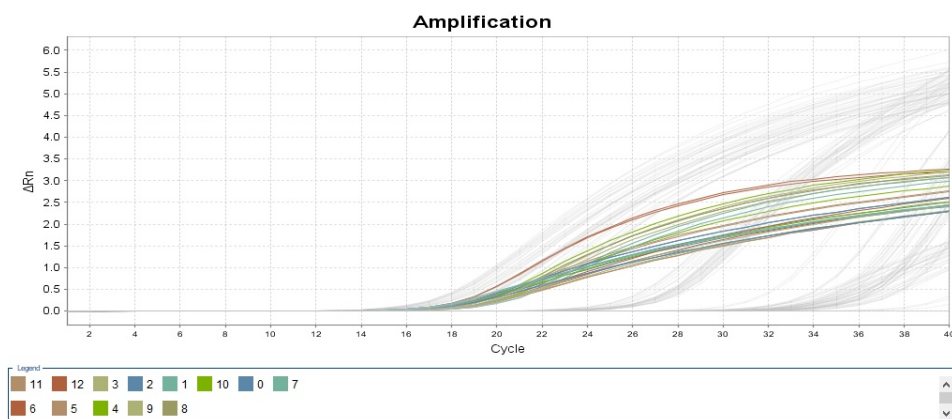


Figure 7.4: COL1A1 Amplification plot, Experiment 1

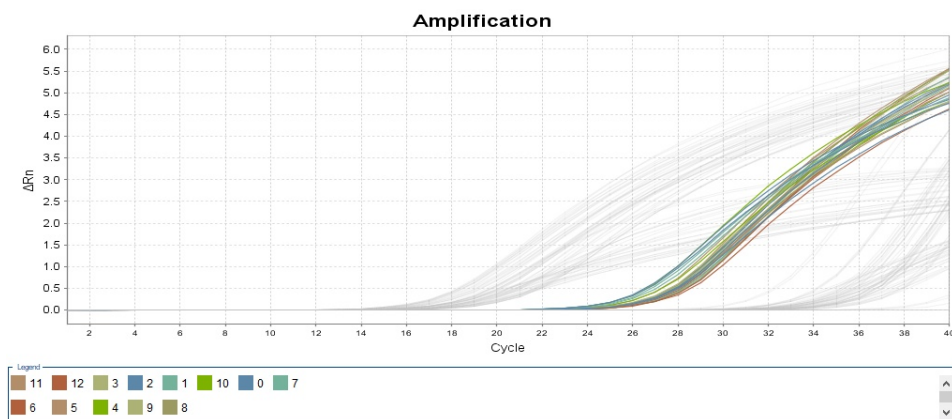


Figure 7.5: RUNX2 Amplification plot, Experiment 1

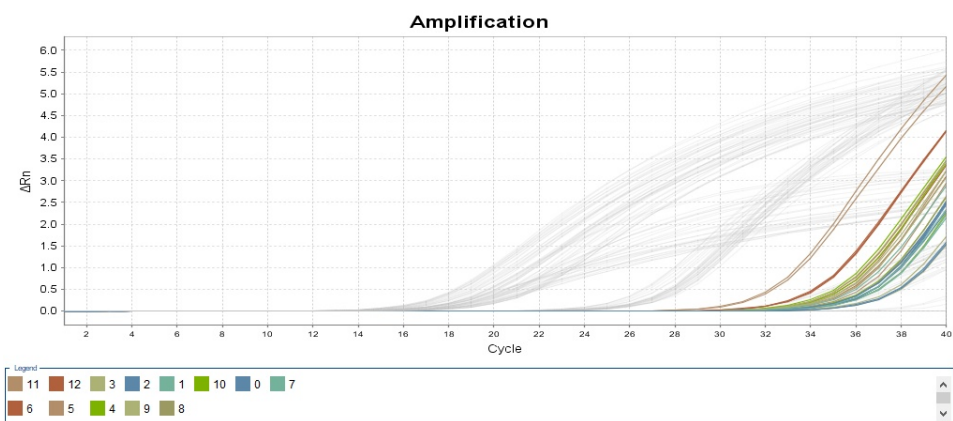


Figure 7.6: SP7 Amplification plot, Experiment 1

Amplification Plots, Experiment 2

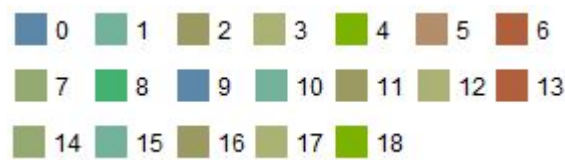


Figure 7.7: Color labeling

#	Name	#	Name	#	Name
1	Blank, D7, OM	7	Large, D7, OM	13	Ti, D7, OM
2	Blank, D7, GM	8	Large, D7, GM	14	Ti, D7, GM
3	Blank, D14, OM	9	Large, D14, OM	15	Ti, D14, OM
4	Blank, D14, GM	10	Large, D14, GM	16	Ti, D14, GM
5	Blank, D21, OM	11	Large, D21, OM	17	Ti, G21, OM
6	Blank, D21, GM	12	Large, D21, GM	18	Ti, D21, GM

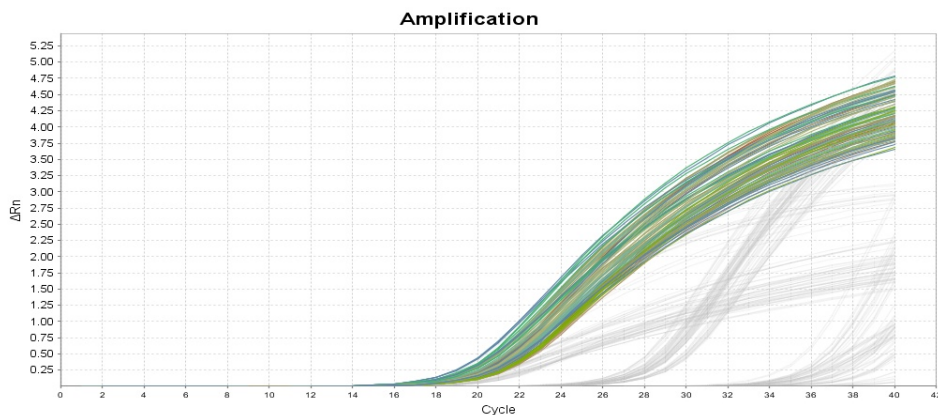


Figure 7.8: GAPDH Amplification plot, Experiment 2

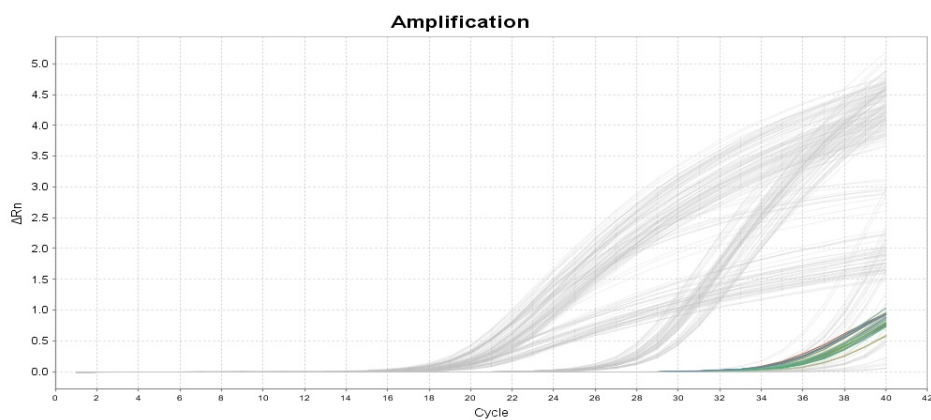


Figure 7.9: BGLAP Amplification plot, Experiment 2

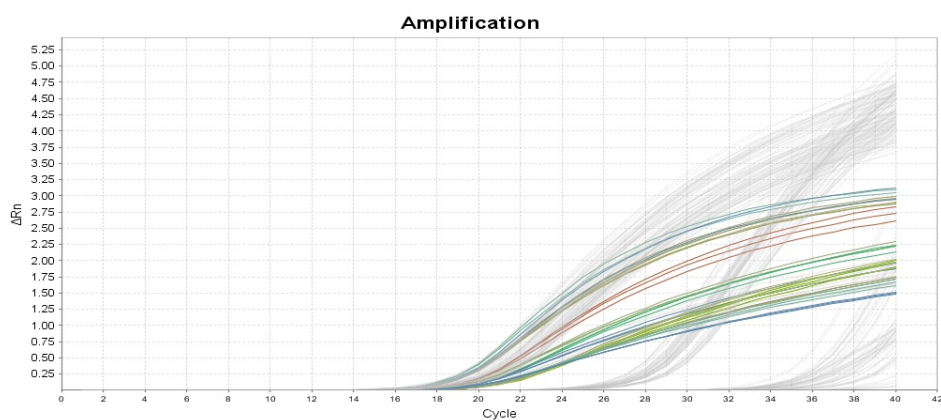


Figure 7.10: COL1A1 Amplification plot, Experiment 2

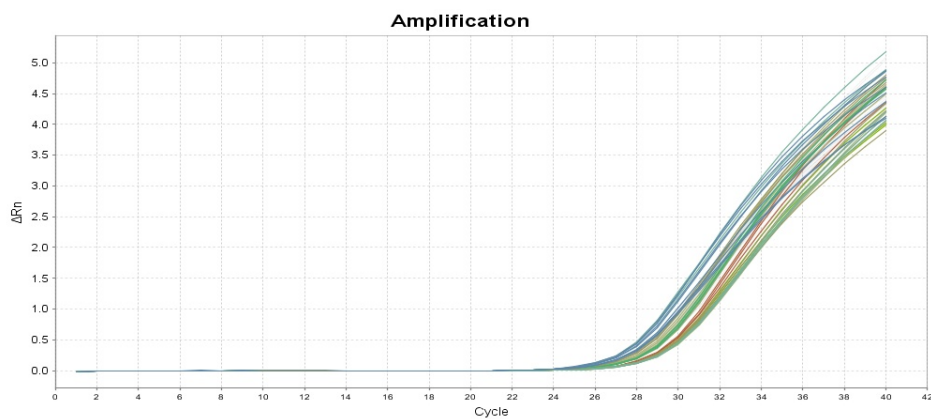


Figure 7.11: RUNX2 Amplification plot, Experiment 2

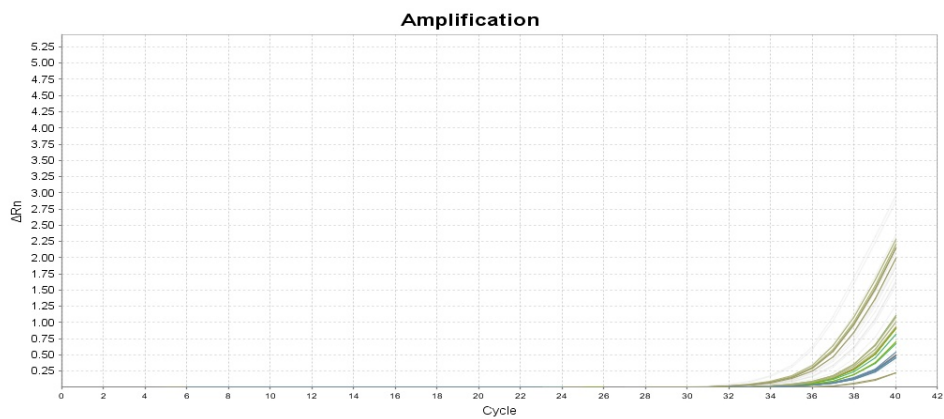


Figure 7.12: SP7 Amplification plot, Experiment 2

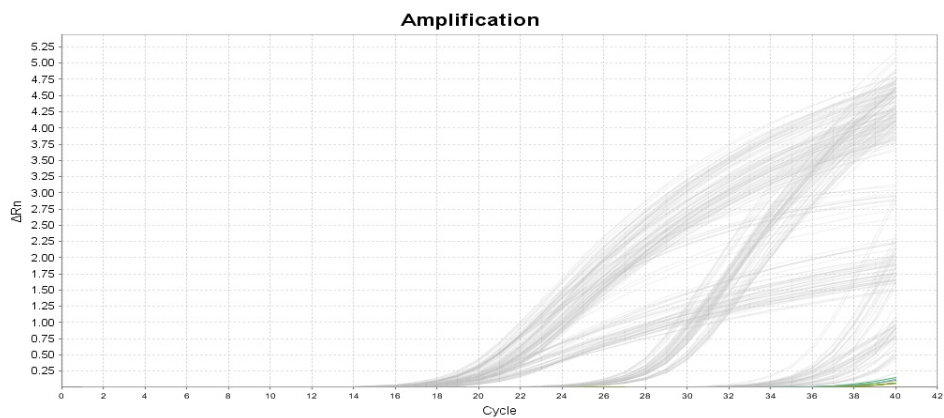


Figure 7.13: SOST Amplification plot, Experiment 2